Environmental Flow Impacts on Tropical Cyclone Structure Diagnosed from Airborne Doppler Radar Composites

PAUL D. REASOR AND ROBERT ROGERS

Hurricane Research Division, NOAA/Atlantic Oceanographic and Meteorological Laboratory, Miami, Florida

SYLVIE LORSOLO

Hurricane Research Division, NOAA/Atlantic Oceanographic and Meteorological Laboratory, and Cooperative Institute for Marine and Atmospheric Studies, University of Miami, Miami, Florida

(Manuscript received 19 November 2012, in final form 5 March 2013)

ABSTRACT

Following a recent demonstration of multicase compositing of axisymmetric tropical cyclone (TC) structure derived from airborne Doppler radar measurements, the authors extend the analysis to the asymmetric structure using an unprecedented database from 75 TC flights. In particular, they examine the precipitation *and* kinematic asymmetry forced by the TC's motion and interaction with vertical wind shear. For the first time they quantify the average magnitude and phase of the three-dimensional shear-relative kinematic asymmetry of observed TCs through a composite approach. The composite analysis confirms principal features of the shear-relative TC asymmetry documented in prior numerical and observational studies (e.g., downshear tilt, downshear-right convective initiation, and a downshear-left precipitation maximum). The statistical significance of the composite shear-relative structure is demonstrated through a stratification of cases by shear magnitude. The impact of storm motion on eyewall convective asymmetry appears to be secondary to the much greater constraint placed by vertical wind shear on the organization of convection, in agreement with prior studies using lightning and precipitation data.

1. Introduction

Forecasting of tropical cyclone (TC) intensity remains a great challenge in which the gains in skill over the past decade have significantly lagged those of track at most forecast intervals (Rogers et al. 2006, DeMaria et al. 2005). As a multiscale atmospheric and oceanic problem, one of the constraints on TC intensity change is the vortex's interaction with the evolving environmental flow. Vertically sheared flow in particular is generally acknowledged to limit storm intensity, especially when combined with other environmental factors like low sea surface temperature and midtropospheric dry air (e.g., Tang and Emanuel 2012). One of the earliest ideas to explain this impact of shear on intensity invoked midlevel ventilation of the eyewall (Simpson and Riehl 1958). Frank and Ritchie (2001) argued for weakening via the development of convective asymmetry followed by outward fluxes of upper-level potential vorticity and equivalent potential temperature θ_e. Alternatively, DeMaria (1996) suggested that vertical tilting of the TC vortex could yield a more stable stratification in the lower to midtroposphere, which in turn would weaken eyewall convection. Riemer et al. (2010) have recently critiqued the various theories for shear-induced intensity modification and offered a new paradigm focusing on a mechanism, connected to the asymmetric balance vortex dynamics, for introducing cooler and drier (lower θ_e) air into the storm's inflow layer.

We currently lack a complete set of observations with which to test the aforementioned theories on a single-case basis. A limited number of observational studies, however, have focused on aspects of the shear-relative kinematic and precipitation structure of individual TCs (e.g., Reasor et al. 2000; Black et al. 2002; Reasor et al. 2009; Reasor and Eastin 2012, hereafter RE12). Using vertical incidence radar data within two sheared TCs, Black et al. (2002) constructed cross sections of eyewall reflectivity and vertical wind. Their summary schematic

Corresponding author address: Paul D. Reasor, Hurricane Research Division, NOAA/Atlantic Oceanographic and Meteorological Laboratory, Miami, FL 33149.
E-mail: paul.reasor@noaa.gov

DOI: 10.1175/MWR-D-12-00334.1

illustration of shear-induced convective asymmetry depicts convective initiation in the downshear quadrant. To the left of shear, buoyant updrafts accelerate, and a maximum in precipitation occurs. On the upshear side of the eyewall, they argued that lower- to midtropospheric downdrafts are enhanced through evaporative cooling and condensate loading. Glaciated updrafts continue around the semicircle right of shear and ascend through the upper troposphere, producing an exhaust anvil.

A complementary study of sheared TC structure and evolution conducted by RE12 used radar-derived wind fields and flight-level thermodynamic measurements to document relationships between shear, vortex tilt, and associated asymmetry within the core region.[1] For deep-layer shear values approaching $10\,m\,s^{-1}$, the TC in their study remained vertically resilient, and a concomitant rapid intensification occurred. They found that the TC tilted preferentially to the left of shear, as is common in idealized and case studies of simulated storms (Wang and Holland 1996; Braun and Wu 2007; Davis et al. 2008; Riemer et al. 2010) and predicted by analytic models (Reasor et al. 2004). A thermal asymmetry within the eyewall was observed oriented along the tilt direction, consistent with the expectations of asymmetric balance dynamics (Jones 1995; Braun et al. 2006). Composite eyewall ascent was maximized close to the downtilt direction, which also coincided with the quadrant of enhanced low-level, storm-relative inflow (cf. Bender 1997; Rogers et al. 2003; Braun et al. 2006; Wu et al. 2006; Davis et al. 2008).

Observational studies have also employed multicase composite and statistical methods to diagnose the impacts of shear on TC structure. Many of these studies have sought to distinguish the shear-induced contribution to storm asymmetry from that associated with other mechanisms (e.g., storm translation). Using lightning data from the National Lightning Detection Network (NLDN) as a proxy for deep convection, Corbosiero and Molinari (2002, 2003, hereafter CM02 and CM03, respectively) found that flashes occur preferentially within the downshear-left quadrant of the core region. When cases were composited relative to the direction of storm motion, a preference for flashes in the front-right quadrant was observed. However, a systematic relationship between shear and motion also existed in their dataset with the motion vector typically left of the deep-layer shear. Based upon a stratification of cases according to the angle between motion and shear vectors, they concluded that the shear-induced forcing dominates the motion-induced forcing of deep convective asymmetry within the core region. Subsequent multicase analyses of shear-induced TC asymmetry using satellite-based precipitation estimates have confirmed a downshear to downshear-left preference for rainfall (Chen et al. 2006; Cecil 2007; Ueno 2007; Wingo and Cecil 2010; Hence and Houze 2011). Motion impacts on the distribution of precipitation in these studies were most clearly observed only for the weakest shear magnitudes. Other multicase studies of sheared TCs have demonstrated shear impacts on the vertical structure of the axisymmetric warm core using microwave brightness temperature (Knaff et al. 2004) and on the azimuthal distribution of near-core helicity and convective available potential energy using dropsonde data (Molinari and Vollaro 2010).

A primary goal of the present paper is to diagnose the impacts of shear on TC structure through shear-relative compositing of both the three-dimensional precipitation *and* kinematic fields. We employ a database of radar-observed storms, made possible through the coordinated annual field program of the National Oceanic and Atmospheric Administration's (NOAA) Aircraft Operation Center (AOC) and Hurricane Research Division (HRD) over the past two decades. Rogers et al. (2012) recently used this database in their composite analysis of axisymmetric TC structure. We extend their kinematic analysis to the asymmetric component of the storm using an expanded database of cases. The data and methodology used to construct the shear-relative composites are discussed in section 2. After a brief overview of axisymmetric and asymmetric structure derived from the database, various aspects of shear-relative TC asymmetry are presented in section 3. In addition, we offer some evidence supporting the finding of previous studies that shear forcing tends to dominate motion forcing of deep convective asymmetry. Conclusions and future directions for further exploration of shear-induced TC intensity change using the radar database are discussed in section 4.

2. Methodology

a. Dataset

As in Rogers et al. (2012), composites of core-region structure were created using tail Doppler radar data from NOAA WP-3D aircraft radial penetrations in multiple storms. The database is expanded here to include 75 flights in 19 storms from 1997 to 2010. Figure 1 shows the storm tracks and locations of flights by the

[1] We employ the same dynamically motivated definition of "core" as that used by RE12 to indicate the central region of the vortex with highest vorticity. The eyewall is the region of strongest winds and heaviest precipitation near the edge of the core. The "core region" includes the skirt of greatly reduced positive relative vorticity immediately surrounding the core.

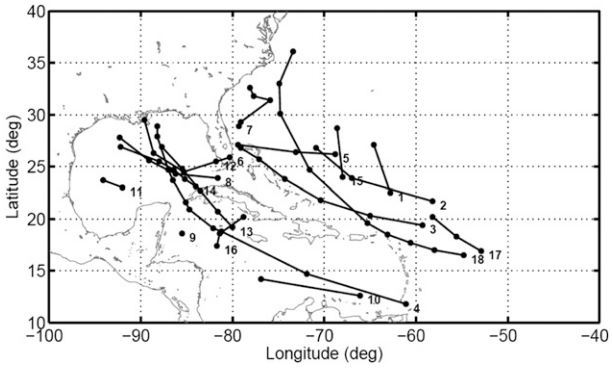

FIG. 1. Storm tracks during NOAA P-3 tail Doppler radar sampling for each case in the current database. Dots denote the center locations of individual flights, and the numbers indicate individual storms. The sole eastern Pacific storm in the database, Hurricane Guillermo (1997), is not shown.

WP-3D aircraft for the periods included in this study. Each of the flights consisted of at least two passes through the core region, yielding a total of 249 radial penetrations. For most flights, the observations were made well away from land, thus limiting the impact of land interaction on the results.

Basic environmental and storm properties of the flights are summarized in Fig. 2. In addition, Table 1 lists the number of cases and mean properties for the entire database and various stratifications examined in section 3. Since the radar data coverage in weaker TCs can be irregular, and the primary circulation sometimes ill defined, the analysis is limited to those flights for which the National Hurricane Center (NHC) best-track intensity $V_{\max}$ exceeds $31\,\mathrm{m\,s^{-1}}$, or approximately hurricane strength (hereafter we refer to hurricanes rather than TCs for clarity). This threshold reduces the total number of viable flights for compositing to 63. The basic environment of these storms is reflected here by the deep-layer shear ($S_{850\text{–}200}$; Fig. 2a), sea surface temperature (SST; Fig. 2b), and storm motion (U_s; Fig. 2c). The 850–200-hPa shear was taken from the Statistical Hurricane Intensity Prediction Scheme (SHIPS) database (DeMaria et al. 2005). The shear is derived from the National Centers for Environmental Prediction (NCEP) operational global model analysis and defined as the vector difference of the mean winds within a 500-km radius of the storm center between 200 and 850 hPa (Kaplan et al. 2010). The shear magnitude generally ranges from 0 to $10\,\mathrm{m\,s^{-1}}$ with a mean value of $5.7\,\mathrm{m\,s^{-1}}$. The shear direction, which is discussed further in section 3d, has a westerly component in a majority of cases. SST (Reynolds and Smith 1993) shows a narrow distribution with a mean value of 29.3°C. The storm motion U_s ranges from 1 to $10\,\mathrm{m\,s^{-1}}$ with a mean value of $5.6\,\mathrm{m\,s^{-1}}$. The mean direction of motion is to the northwest (140°),[2] as can be inferred from Fig. 1.

Some important environmental differences between the current database and that used in the composite study of CM02/CM03 are worth noting. CM02/CM03's use of NLDN data limited cases to those over land or within roughly 400 km of the U.S. coastline. The average motion of their storms was to the north-northeast, consistent with recurving TCs. Their average shear was to the east-northeast at $9.3\,\mathrm{m\,s^{-1}}$ with a primary peak between 11 and $12\,\mathrm{m\,s^{-1}}$. A secondary peak in the 5–8 $\mathrm{m\,s^{-1}}$ range is consistent with the primary peak of the shear distribution here. The greater frequency of high-shear cases in CM02/CM03's database reflects a greater number of higher-latitude storms.

The basic vortex is characterized here by the NHC best-track intensity ($V_{\max}$; Fig. 2d), maximum azimuthal-mean tangential wind at 2 km ($V_{2\mathrm{km}}$; Fig. 2e), and radius of $V_{2\mathrm{km}}$ ($\mathrm{RMW}_{2\mathrm{km}}$; Fig. 2f). The method for computing the azimuthal-mean fields used to derive $V_{2\mathrm{km}}$ and $\mathrm{RMW}_{2\mathrm{km}}$ for each flight is discussed below in section 2b. The majority of cases are classified as major hurricanes ($V_{\max} > 50\,\mathrm{m\,s^{-1}}$). In contrast, the storms of CM02/CM03's database had peak frequency within the tropical depression classification ($V_{\max} < 17\,\mathrm{m\,s^{-1}}$). The distributions here of $V_{\max}$ and $V_{2\mathrm{km}}$ both peak between 50 and $60\,\mathrm{m\,s^{-1}}$. $\mathrm{RMW}_{2\mathrm{km}}$ is strongly peaked between 30 and 45 km.

b. Data quality control and synthesis

The analysis of tail Doppler radar data from such a large number of aircraft radial penetrations was made possible by an automated quality control process (Gamache 2005) and variational wind synthesis method (Gamache 1997; Reasor et al. 2009). In all cases the fore/aft scanning technique was employed in which the radar antenna scans in a cone 20° from the track-normal plane alternately fore and aft of the aircraft. Such a technique yields dual-Doppler measurements from a single radial penetration. The limitations of such a sampling strategy are well documented in prior case studies (e.g., Reasor et al. 2009). The quality-controlled Doppler radials are mapped to a storm-centered 400 km by 400 km Cartesian domain extending from the surface to 20-km height with horizontal and vertical grid spacing of 2 and 0.5 km, respectively. The Doppler radar projection equations and anelastic mass continuity equation are then solved simultaneously for the three-dimensional wind field via least squares minimization.

[2] A mathematical angle convention is employed throughout with 0° denoting east, 90° denoting north, etc.

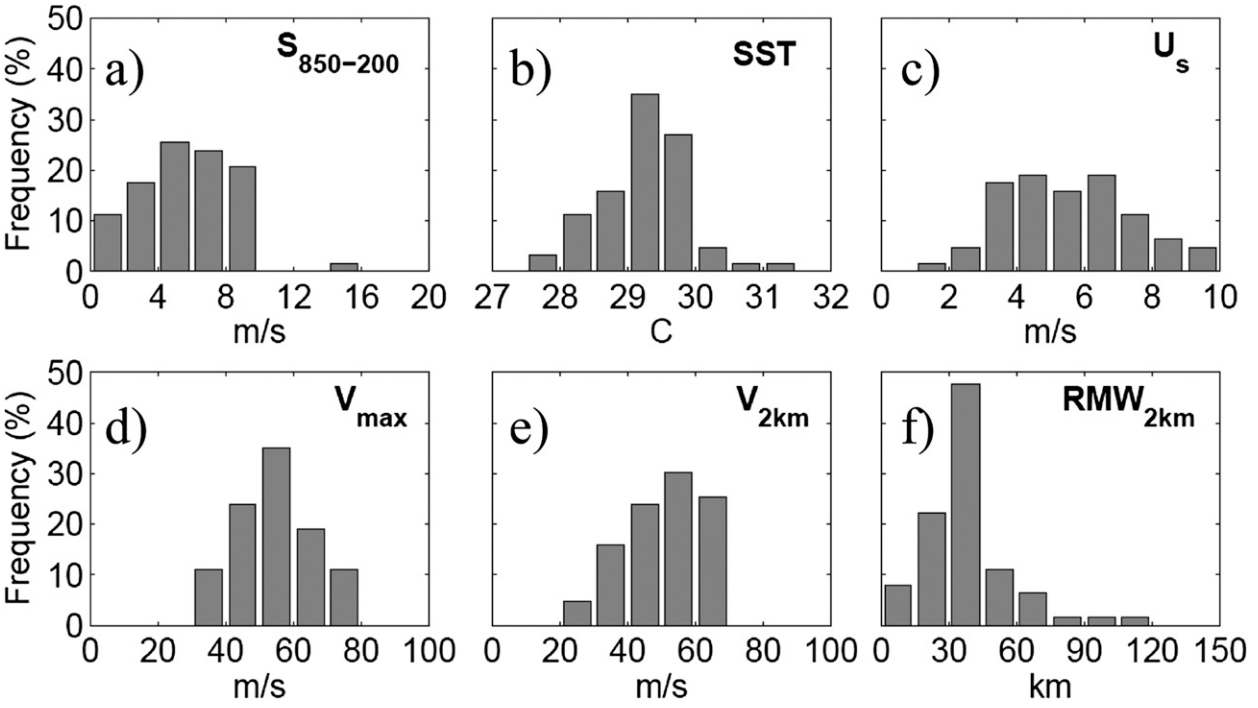

FIG. 2. Distribution of basic environmental and storm parameters for cases with $V_{max} > 31\ m\ s^{-1}$. (a) SHIPS 850–200-hPa vertical shear, (b) Reynolds sea surface temperature, (c) storm speed, (d) NHC best-track intensity, (e) maximum azimuthal-mean tangential wind at 2 km, and (f) RMW at 2 km.

The primary metrics used to characterize the impacts of environmental flow on hurricane structure include the axisymmetric and azimuthal wavenumber-1 fields, vortex center tilt, and local shear. Following RE12, the vortex center is defined using a modified version of the center-finding method of Marks et al. (1992). The method seeks the center, which maximizes the annulus-average tangential wind on the scale of the radius of maximum wind (RMW), carefully accounting for gaps in the wind field. The local shear was derived from the area average of wind within 80 km of the local vortex center at each height.[3] For the purpose of azimuthal Fourier analysis, the Cartesian data were mapped to a cylindrical coordinate system centered on the vortex at 2-km height with radial and azimuthal grid spacing of 2 km and 5°, respectively. Because of limited data coverage for some radial penetrations, and the subjective coverage thresholds introduced to ensure robust estimates, not all metrics could be computed at all heights.

Since the focus here is on structural features of the hurricane that evolve with the environment on a time scale longer than the intensive observation period (~3–4 h), analyses from individual radial penetrations are merged over a flight. The merger entails a simple average of wind and reflectivity (dBZ) at overlapping storm-relative grid points. Figure 3 shows an example merged analysis of wind speed from a recent flight into Hurricane Earl (2010). The analysis from each radial penetration, henceforth referred to as a ''swath,'' is at most 90 km across with variations in width along the flight track typically resulting from attenuation, changes in the fore/aft beam geometry, and radar sensitivity. Since reflectivity does not require dual measurements to produce an analysis, its coverage will be greater than that of the wind field.

c. Compositing methodology

Shear- and motion-relative composites of core-region reflectivity and kinematic fields for hurricanes are created here to extend the composite studies of lightning and precipitation discussed in the introduction. In addition, these multicase composites confirm the significant features of sheared storms identified in prior case studies. Since the radial scale of the core region varies from case to case, the horizontal dimension of each analysis is scaled by RMW_{2km}, similar to that done in Rogers et al. (2012). The normalized radius r^* is defined by $r^* = r/RMW_{2km}$ and the normalized Cartesian coordinates

[3] The method for radar-based shear estimation outlined in RE12 is followed here. Given adequate data coverage to define and remove the azimuthal-mean circulation, the shear is computed by differencing the vortex-centered, area-average winds at two heights.

TABLE 1. Mean values of basic environmental and vortex parameters for the different stratifications examined with $V_{max} > 31\,m\,s^{-1}$. The environment is characterized here by the deep-layer shear ($S_{850–200}$), sea surface temperature (SST), and storm motion (U_S). The vortex is characterized by the NHC best-track intensity (V_{max}), maximum azimuthal-mean tangential wind at 2 km (V_{2km}), and radius of V_{2km} (RMW_{2km}).

Stratification	No. of cases n	$S_{850–200}$ ($m\,s^{-1}$)	SST (°C)	U_S ($m\,s^{-1}$)	V_{max} ($m\,s^{-1}$)	V_{2km} ($m\,s^{-1}$)	RMW_{2km} (km)
All	63	5.7	29.3	5.6	54.6	49.7	39
$S_{850–200} > 2.5\,m\,s^{-1}$	52	6.6	29.3	5.8	53.5	48.7	39
$S_{850–200} < 4\,m\,s^{-1}$	18	2.1	29.1	5.3	56.9	51.5	37
$S_{850–200} > 7\,m\,s^{-1}$	22	8.7	29.3	6.3	55.1	51.3	44
shear 90°–180° left of motion	14	5.2	29.3	5.0	53.5	48.0	35
shear 90°–180° right of motion	16	6.4	29.3	5.2	55.5	50.5	44

(X^*, Y^*) are defined by (X^*, Y^*) = (X, Y)/RMW_{2km}. To ensure a common reference center for the compositing, the Cartesian and cylindrical domains of each analysis are defined with their origins at the 2-km vortex center. The storm translation is then removed from each wind analysis to yield storm-relative winds. In the final step before compositing, all fields are rotated such that the motion vector or SHIPS deep-layer shear vector points in the positive x direction. In the case of shear-relative composites, we divide the storm into quadrants listed here in counterclockwise order: downshear right (DSR), downshear left (DSL), upshear left (USL), and upshear right (USR). Stratifications based on hurricane intensity, shear magnitude, and the direction of motion and shear are discussed below.

3. Results

a. General axisymmetric and asymmetric characteristics

The composite analysis of axisymmetric structure presented in Rogers et al. (2012) confirmed features of the hurricane commonly observed in case studies (e.g., Marks and Houze 1987; Marks et al. 1992). Figure 4 shows normalized radial profiles of axisymmetric tangential wind and vorticity at 2 km for the expanded database here. While the tangential wind decays radially outside $r^* = 1$ in most cases, the rate at which it does so varies considerably (Fig. 4a). Distinct secondary wind maxima are evident in a few cases, three of which exceed the identified primary maximum at $r^* = 1$. Since the inner and outer peak tangential wind values are close, and the data distribution is sparse for the outer maximum in these special cases, the well-resolved inner maximum was chosen to scale the vortex. Weaker inner wind maxima are also evident in a few cases. The composite vorticity profile outside the core decreases monotonically with increasing radius (Fig. 4b). Secondary vorticity maxima are generally consistent with cases having a pronounced outer wind maximum. In most cases, a well-defined vorticity skirt surrounds the higher vorticity core, as documented in Mallen et al. (2005) using flight-level measurements.

Deviations from axisymmetry are often stochastically forced on the convective scales (e.g., Nguyen et al. 2008), but can also result from internal dynamical mechanisms and external forcing. Therefore, a composite approach to characterizing asymmetry of the hurricane core region must be carefully constructed. For example, in the case of rotating elliptical eyewalls, one might composite relative to the ellipse's major axis. In the composite

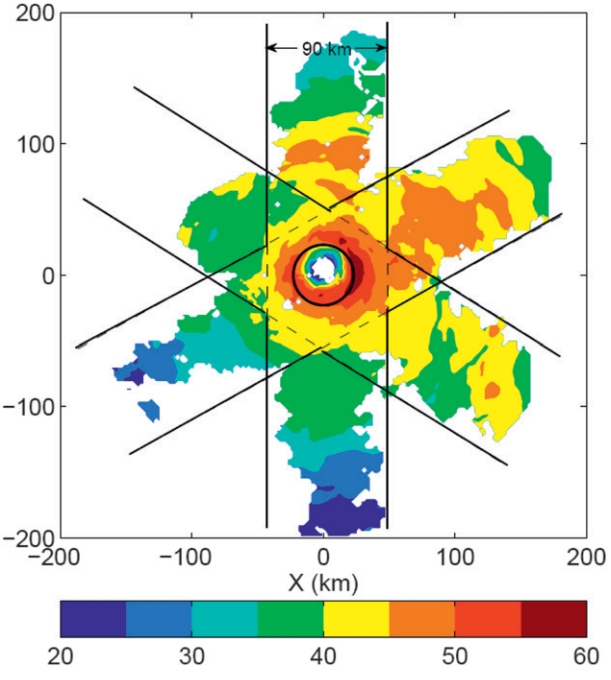

FIG. 3. Storm-relative wind speed ($m\,s^{-1}$) at 2 km from the 2049 to 2404 UTC 30 Oct 2010 merged analysis of Hurricane Earl. Solid lines denote approximate boundaries of useable wind data for each of the three individual eyewall passes. Dashed lines bound the region of significant overlap between passes. RMW_{2km}, denoted by the solid circle, falls entirely within the region of significant overlap in this case.

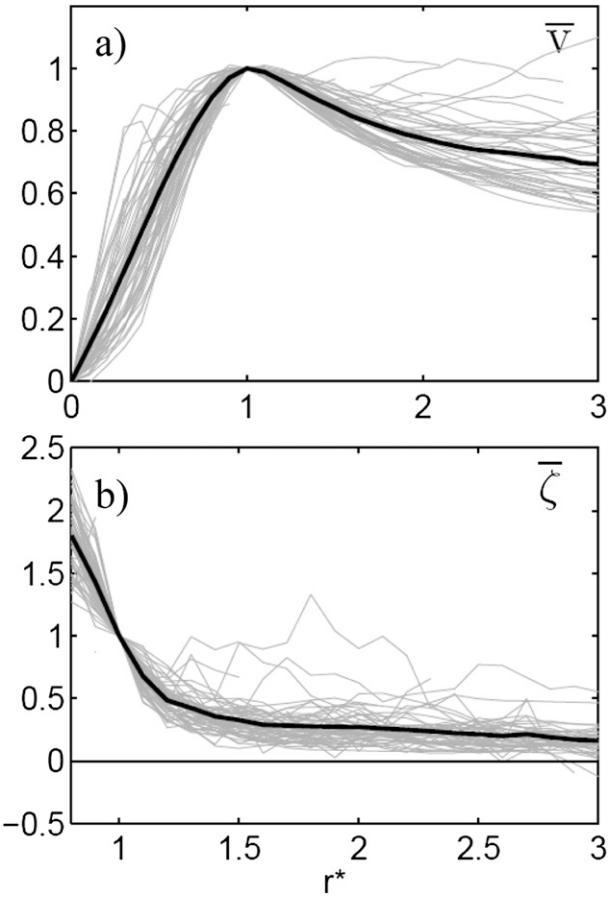

FIG. 4. Radial profiles of (a) azimuthal-mean tangential wind ($m\,s^{-1}$) and (b) relative vorticity (s^{-1}) at 2 km for cases with $V_{max} > 31\,m\,s^{-1}$. The radial coordinate r^* is scaled by RMW_{2km}, and the profiles are normalized by their values at $r^* = 1$. The vorticity is shown only for $r^* > 0.75$ to emphasize the vortex skirt structure. The heavy solid lines denote the mean profiles.

analyses of sections 3b–d, we exploit the fact that the hurricane's structural response to sustained shear and translational forcing can have a pronounced quasi-steady, low-azimuthal-wavenumber component (e.g., Braun et al. 2006; Reasor et al. 2009; Thomsen et al. 2013, manuscript submitted to *Mon. Wea. Rev.*).

As a first step toward assessing the impact of internal and external mechanisms on storm asymmetry across the database, attention is restricted here to the asymmetry amplitude. Axisymmetric storms are discriminated from those that, either through lack of organization or through the influence of internal asymmetry-producing processes, have a high degree of asymmetry through the use of an asymmetry metric:

$$\sigma_{\max}(Q) = \max\left\{\sqrt{\frac{1}{N_i - 1}\sum_{k=1}^{N_i}[Q_k(r_i) - \overline{Q}(r_i)]^2}\right\}_{i=1}^{M},$$

where Q is the field variable (e.g., reflectivity), $[r_1, r_M]$ defines the radial band, N_i is the number of azimuthal data points at $r = r_i$, and the overbar denotes the azimuthal mean. Here $\sigma_{\max}(Q)$ is simply the maximum azimuthal standard deviation of Q from its azimuthal-mean value within the prescribed radial band. Here the radial band coincides with the eyewall, which for each field variable Q is defined approximately as the region where $\overline{Q}$ is maximized.[4] Nguyen et al. (2011) used a similar metric to relate simulated vacillations between axisymmetric and asymmetric eyewall states with intensity change cycles. The distribution of $\sigma_{\max}$ for the eyewall region is shown in Fig. 5. For 2-km vorticity (ζ; Fig. 5a) the eyewall is defined as the $r^* = 0.6$–1.0 band, and the most frequent range of $\sigma_{\max}(\zeta)$ is $0.75–1 \times 10^{-3}\,s^{-1}$. For 5-km vertical velocity (W, Fig. 5b) and 2-km reflectivity (Z, Fig. 5c) the eyewall definition is shifted outward to include the $r^* = 0.8$–1.2 band, and the most frequent range of $\sigma_{\max}(W)$ and $\sigma_{\max}(Z)$ is 1.5–2 $m\,s^{-1}$ and 4–6 dBZ, respectively. Although representation of the eyewall asymmetry is likely to be affected by factors such as the swath merger, nonsimultaneity of Doppler measurements, and the smoothing inherent in the radar analysis methodology (Reasor et al. 2009), the distributions shown in Fig. 5 may be used to provide rough estimates of expected asymmetry amplitude. When the asymmetry metric is computed using only the wavenumber-1 component, we find that the value normalized by $\sigma_{\max}$ is on average 83% for reflectivity and 74% for vertical velocity. For vorticity the normalized value is on average 57%, indicating a greater relative contribution of higher-wavenumber Fourier components to the vorticity asymmetry represented in the merged analyses.

The prominence of the wavenumber-1 component in the eyewall convective field is anticipated when a hurricane interacts with its environment (e.g., Reasor et al. 2009). This relationship, as well as the impact of the environment on the overall kinematic structure of the hurricane, is further explored through the compositing methodology described in section 2c. Since the impact of translational forcing on structure tends to be subtle when shear is present (e.g., CM03), we focus first on the shear-relative hurricane structure.

b. Shear-relative hurricane: Basic structure

When a hurricane is vertically sheared, differential advection of potential vorticity yields a tilted wind structure characterized by a deviation from axisymmetry, referred to here as the tilt asymmetry. In the limit of

[4] The reader is referred to Rogers et al. (2012) for composites of TC azimuthal-mean structure.

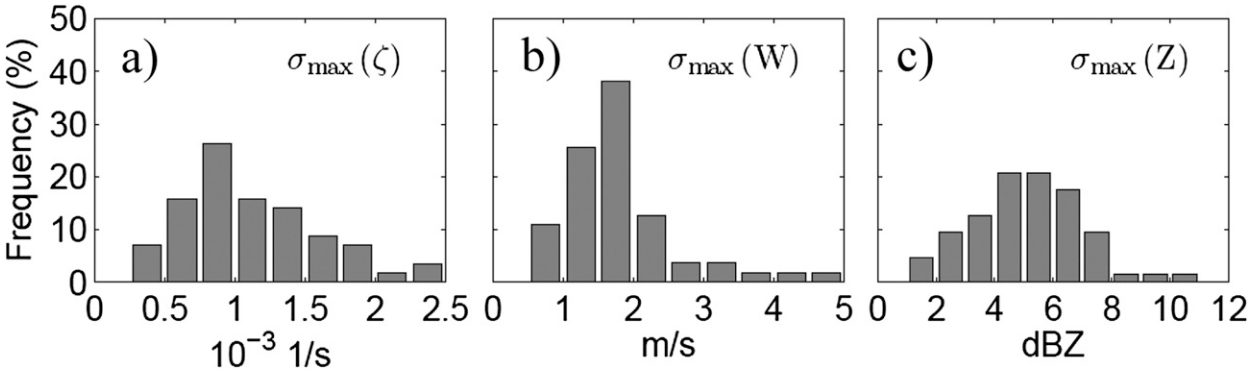

FIG. 5. Distribution of eyewall asymmetry for cases with $V_{max} > 31\,m\,s^{-1}$ as measured by the maximum standard deviation from the azimuthal mean of (a) 2-km vorticity, (b) 5-km vertical velocity, and (c) 2-km reflectivity in the eyewall. See the text for the radial intervals constituting the ''eyewall'' for each variable.

small but finite-amplitude tilt, the tilt asymmetry is meaningfully described as a three-dimensional vortex-Rossby wave (Reasor and Montgomery 2001; Reasor et al. 2004). As such, there is no unique definition of center, or tilt, for a hurricane-like vortex in shear given the complex spatial structure of the tilt asymmetry (Jones 1995; Reasor et al. 2004). The center defined in section 2b is representative of the vortex core (RE12). Although centers are computed through a deep layer of the hurricane, the increasingly sparse data coverage with height, especially above 7 km, yields center estimates that are deemed unreliable in many cases. Because of this limitation, our tilt metric is defined as the displacement vector between the 2- and 7-km height centers.

Hurricane core tilt, rotated such that the shear vector in each case points in the positive x direction, is shown in Fig. 6. To ensure a robust impact of shear on storm structure, only hurricanes for which $S_{850–200} > 2.5\,m\,s^{-1}$ are included here and in subsequent shear-relative results, unless otherwise noted. A total of 52 cases meet both the intensity and shear thresholds (Table 1). In the majority of cases, the hurricane core tilts downshear, consistent with differential advection by the deep-layer environmental shear flow. Interestingly, for the range of shear values in the database, the tilt magnitude and $S_{850–200}$ are not well correlated (explained variance $<0.1\%$, not shown). Figure 6 does suggest that the extreme tilt magnitudes are associated with hurricanes for which V_{max} is less than the mean value ($\sim 55\,m\,s^{-1}$). According to theoretical studies of vortex resilience, a weaker vortex should be more prone to developing large tilt in a given shear flow (Jones 1995, 2004; Reasor et al. 2004). Theoretical studies also indicate a dependence of resilience on the radial gradient of vorticity outside the core within the vortex skirt (Reasor et al. 2004) and on the degree of cloudiness within the core region (Schecter and Montgomery 2007). Further examination of hurricane resilience using observational datasets is reserved for future work.

The composite tilt within the 2–7-km layer is directed downshear with a bias $\sim 10°$ to the left of shear (Fig. 7). The average 2–7-km tilt magnitude is approximately 3 km, resulting in a 31° tilt of the core from the vertical axis. The shear-relative orientation of hurricane tilt has been discussed in theoretical (Jones 1995; Reasor et al. 2004), numerical (Wang and Holland 1996; Rogers et al. 2003; Braun et al. 2006; Wu et al. 2006; Davis et al. 2008; Riemer et al. 2010), and observational (Marks et al.

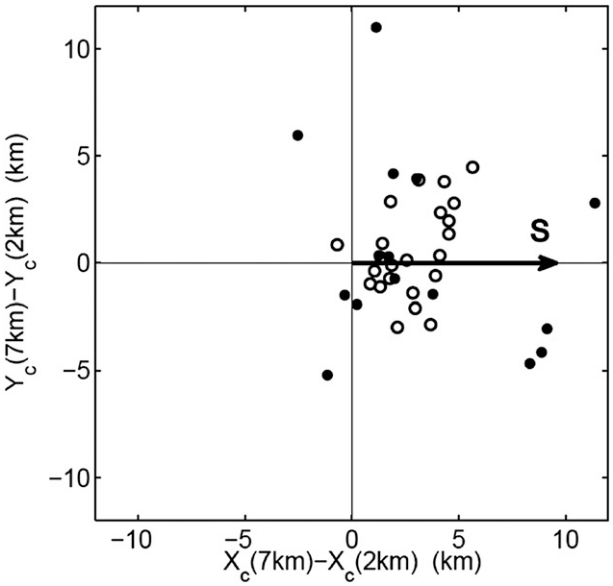

FIG. 6. Shear-relative 2–7-km vortex center (X_c, Y_c) tilt for cases with $V_{max} > 31\,m\,s^{-1}$ and $S_{850–200} > 2.5\,m\,s^{-1}$. Filled (open) circles denote cases in which V_{max} is less (greater) than the population mean value ($\sim 55\,m\,s^{-1}$). In this and all subsequent figures, the direction of large-scale shear is indicated by ''S''.

1992; RE12) studies. According to the dry, balance theory for vortex alignment of Reasor et al. (2004), the tilt of an initially barotropic vortex with hurricane-like radial structure will asymptote to a 90° left-of-shear orientation when forced by unidirectional shear. The vast majority of the aforementioned convection-permitting studies confirm that the vortex generally tilts to the left of shear, although the orientation ranges from downshear to 90° left of shear.

When comparing simulated and observed hurricane tilt to theoretical predictions, or even simply comparing shear-relative studies, it is important to recognize that shear is generally horizontally inhomogeneous (e.g., Jones 2004; Wong and Chan 2004; Dunion and Velden 2004). In cases where the shear direction varies considerably with the scale of the averaging domain, a more local shear is arguably the most relevant to the forcing of vortex tilt. In defining the local averaging scale, one must account for the possibility, as hypothesized by Riemer et al. (2010), that the vortex modifies its local environment through the axisymmetrization process. Directional changes with height of the area-averaged hodograph, and the layer over which one estimates the shear, will also contribute to variability in the phase relationship between tilt and shear (e.g., RE12). In most of the aforementioned numerical studies, a deep-layer local shear is used as a reference. In the observational case study of RE12, the deep-layer local shear derived from radar measurements was similar in direction to the SHIPS large-scale shear. The tilt in that case was ~60° left of shear on average. The direction of composite 2–9-km local shear[5] derived from the radar analyses here is shown in Fig. 7. The local deep-layer shear is ~40° to the right of the SHIPS shear. The composite tilt in this framework is then ~50° to the left of the local shear. Despite this difference, we will continue to reference structure relative to the large-scale shear, but note that a more direct comparison with select prior studies may require reference to the local shear direction instead.

Another leading-order impact of shear on hurricane structure is the generation of convective asymmetry. The azimuthal distribution of shear-relative convective activity, motivated by the lightning-based estimate in CM03 (their Fig. 7a), is examined here using vertical wind and reflectivity data. The core region is first divided into eyewall ($0.8 < r^* < 1.2$) and vortex skirt ($1.5 < r^* < 2.5$) bands. In most cases, the skirt falls within CM02/CM03's ''inner core'' region (i.e., $r < 100$ km).

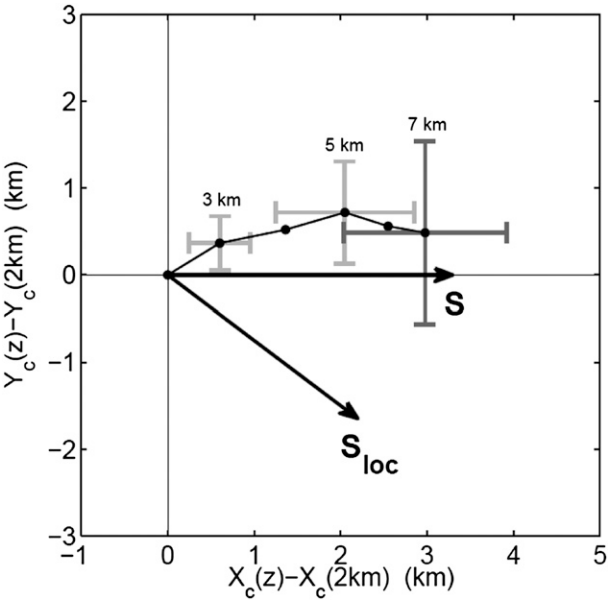

FIG. 7. Shear-relative composite of vortex center (X_c, Y_c) tilt at 1-km height intervals through 7 km for the total population shown in Fig. 6. The tilt structure for each contributing case is referenced to the center at 2 km. The 95% confidence intervals (bars in x and y) are shown at 3, 5, and 7 km. The radar-estimated 2–9-km local shear is indicated by S_{loc} (not to scale).

Within each shear-relative octant of the eyewall, the area of $W > 2.5\,\mathrm{m\,s^{-1}}$ is computed at 5-km height. A similar computation of area for $Z > 35$ dBZ at 2-km height is also made. These thresholds define our estimate of the convective area for the respective fields. They were subjectively determined through visual inspection of the fields in each case so as to provide discrimination between octants, but not so high as to emphasize intense isolated cells. For each case, the octant containing the peak convective area is noted. This analysis approach is repeated for the vortex skirt, but with a lower threshold of $W > 1.5\,\mathrm{m\,s^{-1}}$. The sparser data coverage within the skirt in many cases prohibits octant resolution, so quadrants are considered there.

Figure 8 shows the number of cases in which the peak shear-relative convective area for vertical velocity (Fig. 8a) and reflectivity (Fig. 8b) occurs within a particular octant or quadrant. Within the eyewall, the greatest area of vigorous ascent occurs most frequently in the octant immediately left of shear. Within the skirt, the greatest area of vigorous ascent is confined primarily to the DSL quadrant. As would be expected from hydrometeor production within the most vigorous updrafts, the peak area of elevated low-level reflectivity in both the eyewall and skirt is found within or downwind of the octant and quadrant containing the most frequent peak ascent area. In both the eyewall and skirt, the peak

[5] A slightly deeper layer would better represent the 850–200-hPa shear, but increasingly sparse data coverage with height limits meaningful area averages of wind above 9 km.

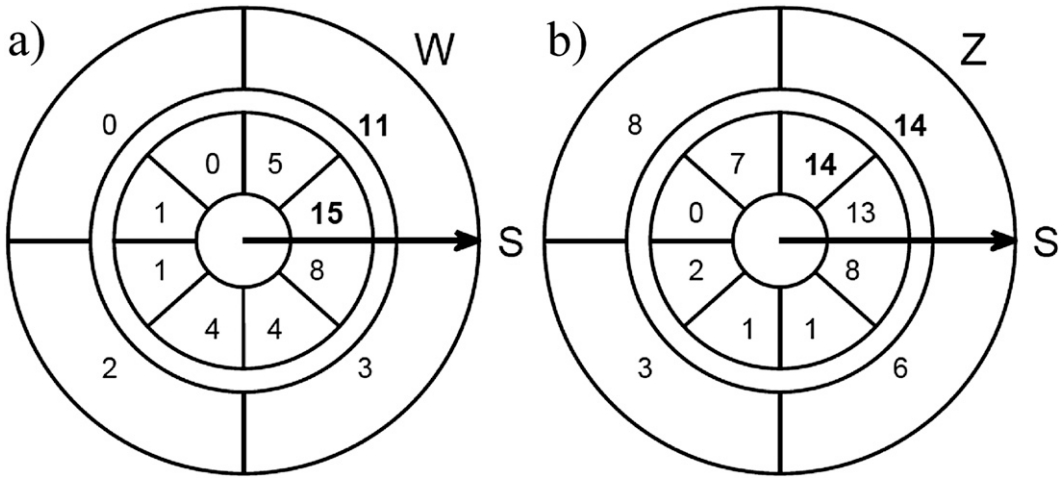

FIG. 8. Number of cases with $V_{max} > 31\,m\,s^{-1}$ and $S_{850-200} > 2.5\,m\,s^{-1}$ in which the peak shear-relative convective area of (a) 5-km vertical velocity and (b) 2-km reflectivity (dBZ) occurred within a given octant of the eyewall region (inner values) and quadrant of the vortex skirt (outer values). See text for the radial intervals constituting the "eyewall" and "vortex skirt" for each variable. The convective area for vertical velocity (reflectivity) is defined by the region with values exceeding $2.5\,m\,s^{-1}$ (35 dBZ) in the eyewall and $1.5\,m\,s^{-1}$ (35 dBZ) in the vortex skirt. Note that inadequate coverage in some cases leads to a reduced total count, particularly within the vortex skirt.

reflectivity is most likely to be observed in the DSL quadrant. The above findings for mature hurricanes are broadly consistent with those of CM02/CM03 for weaker TCs.

The downshear preference for vortex tilt and convective activity motivates shear-relative compositing of the kinematic and reflectivity fields. While the distributions in Figs. 6 and 8 indicate some variance in tilt direction and convective activity relative to the shear direction, the composite analysis will reveal features of the sheared hurricane that have previously been cited in case studies as being physically significant. An advantage of the current approach is that statistical significance can also be assessed.

Shear-relative composites of wind, divergence, and vorticity at 2- and 7-km height are shown in Fig. 9. For plotting, at least 40% of the cases must contribute to the average at a point. The 2-km wind speed (Fig. 9b) is maximized within the DSL quadrant. The wind vectors associated with the asymmetric component (defined relative to the 2-km center) show that this departure from axisymmetry is primarily due to a storm-relative flow approaching (exiting) the eyewall at low levels within the DSR (USL) quadrant. At 7 km (Fig. 9a) the storm-relative asymmetric flow approaches (exits) the eyewall from the upshear (downshear) side. Because of the downshear tilting of the composite vortex, a cross-center asymmetric flow in the right-of-shear direction is superposed on this storm-relative flow inside the eyewall region. Note that the deep-layer shear of the storm-relative asymmetric flow (outside the eyewall) is consistent with the radar-estimated local shear shown in Fig. 7.

The structure of the vorticity asymmetry within the core region is influenced by several mechanisms, including random generation on the convective scales (Nguyen et al. 2008), vortex Rossby wave propagation (Montgomery and Kallenbach 1997), production within spiral rainbands (May and Holland 1999), vortex tilting (Jones 1995; Reasor et al. 2004), dynamic instability (Schubert et al. 1999; Kossin and Schubert 2001; Nolan et al. 2001), and motion-related forcing (Bender 1997). At 2-km height, the composite vorticity asymmetry within $r^* = 1$ exhibits a complex pattern of elevated positive and negative values (Fig. 9d). RE12 argued that a quasi-steady, shear-relative contribution to vorticity asymmetry may arise through vortex stretching within the convectively active downshear eyewall. The elevated positive vorticity downshear in the composite may reflect such convective enhancement, but the variance (not shown) is too large to classify the structures as robust features of the shear-relative hurricane. The shear-relative composite vorticity asymmetry at 7 km (Fig. 9c) takes on a wavenumber-1 structure oriented along the tilt direction indicated in Fig. 7, and is thus readily identified with tilting of the core region. Also of interest is the extension of the tilt asymmetry outside the core identified in dry dynamical models (Jones 1995; Reasor et al. 2004), which has the potential to organize convection on a broad scale outside the eyewall (Riemer et al. 2010). The composite shear-relative vorticity asymmetry at 2 km (Fig. 9d) shows a weak preference for positive

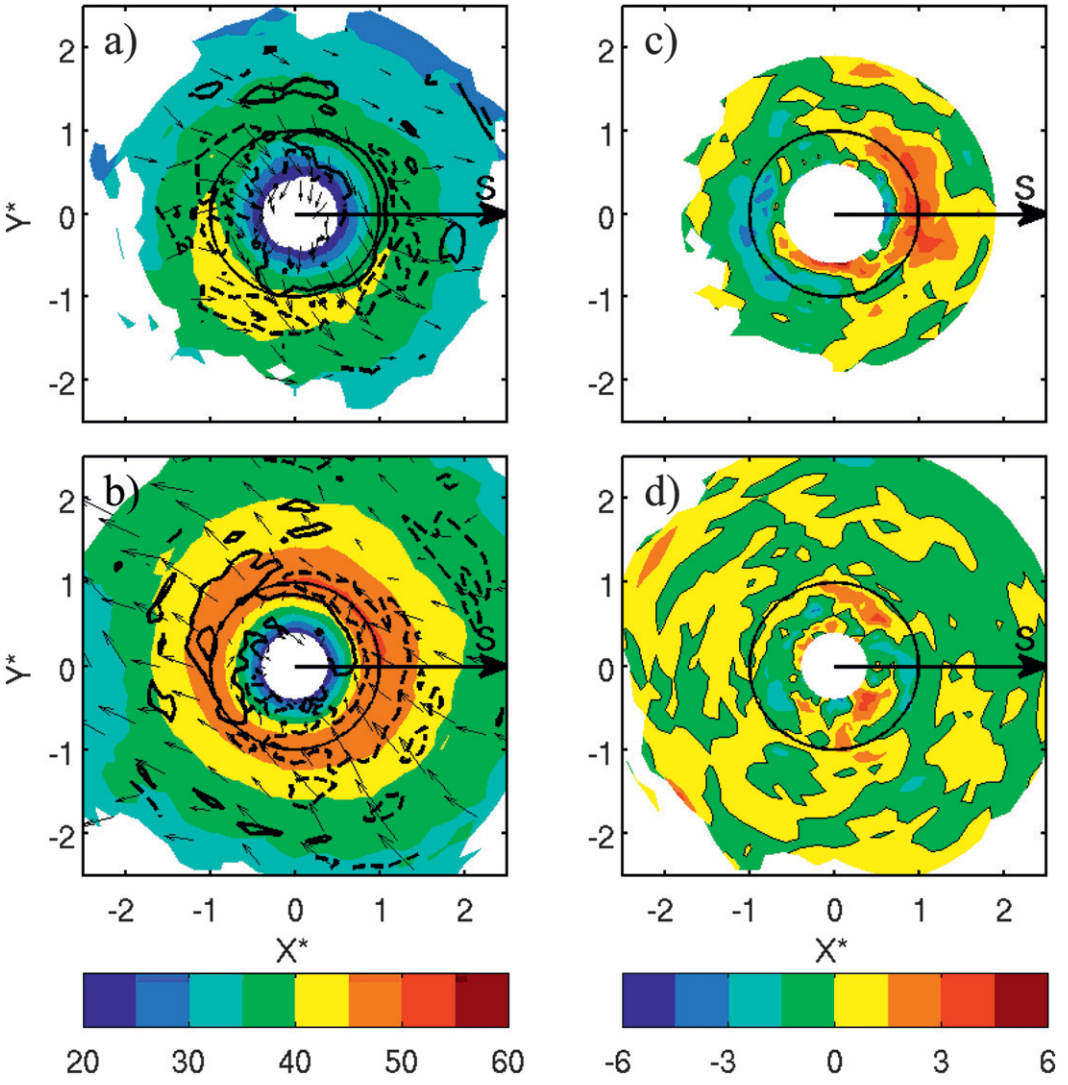

FIG. 9. Shear-relative composite of (a),(b) storm-relative wind speed ($m\,s^{-1}$, shaded) and (c),(d) asymmetric vorticity ($10^{-4}\,s^{-1}$) at (bottom) 2 km and (top) 7 km for cases with $V_{max} > 31\,m\,s^{-1}$ and $S_{850-200} > 2.5\,m\,s^{-1}$. Also shown in (a),(b) are the asymmetric wind vectors and divergence ($10^{-4}\,s^{-1}$, contour). Divergence is contoured only at -1 and $1 \times 10^{-4}\,s^{-1}$ to emphasize regions of positive (solid) and negative (dashed) value. The zero value of asymmetric vorticity is indicated by the solid contour in (c),(d). Horizontal distance (X^*, Y^*) is scaled by RMW_{2km} with $r^* = 1$ denoted by the circle.

vorticity on the uptilt side of the vortex outside the core. The greater complexity of the shear, moisture distribution, and vortex structure (e.g., secondary eyewalls) represented across the database complicates a straightforward comparison with the results of dry and moist idealized simulations. While a broadscale tilt asymmetry should, in principle, be forced through the differential advection of skirt vorticity by the shear flow, new observational strategies and refined analysis techniques may be needed to clearly define it.

The shear-relative asymmetry in composite vertical motion and reflectivity within the eyewall (Fig. 10) is consistent with Doppler vertical incidence cross sections through sheared storms discussed in Black et al. (2002).[6] The region of peak composite ascent is closely aligned with the downshear direction, which also approximately

[6] Black et al. (2002) associated the direction of shear with a local radar estimate. To best relate their analysis to the present composite analysis, the downshear direction would be identified approximately 40° to the right of that defined here. It should be noted, however, that for highly curved local hodographs, the direction of low-level area-average flow and the direction of local deep-layer shear may not coincide.

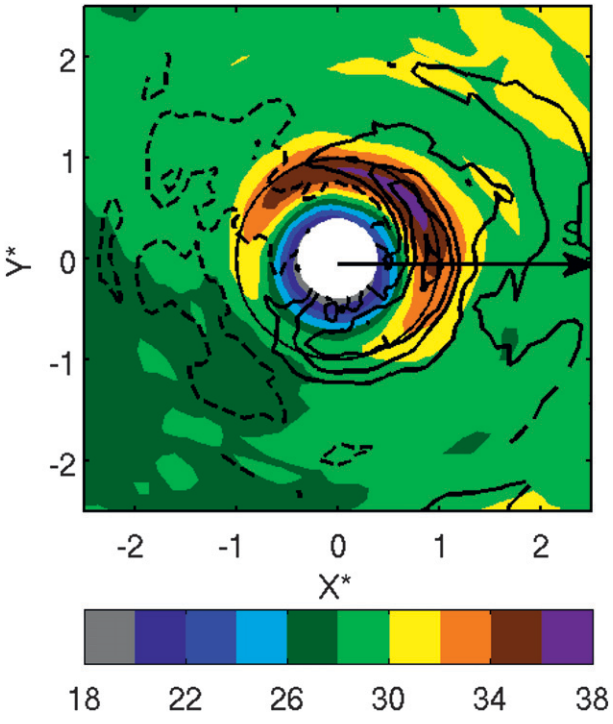

FIG. 10. Shear-relative composite of 2-km reflectivity (dBZ, shaded) and 5-km vertical velocity ($m\,s^{-1}$, contour) for cases with $V_{max} > 31\,m\,s^{-1}$ and $S_{850-200} > 2.5\,m\,s^{-1}$. Negative values of vertical velocity are bounded by the dashed contour. Positive values (solid) are contoured from $0.5\,m\,s^{-1}$ at an interval of $0.5\,m\,s^{-1}$. Horizontal distance (X^*, Y^*) is scaled by RMW_{2km} with $r^* = 1$ denoted by the circle.

coincides with the direction of vortex tilt. The azimuthal distribution of composite ascent is skewed toward the DSR quadrant of enhanced low-level inflow (Fig. 9b). One explanation for the shear-induced convective asymmetry is based upon the dry, balanced dynamical evolution of vortex tilt, first discussed in the TC context by Jones (1995). A vortex under the influence of shear initially develops balanced mesoscale lifting downshear. With the development of tilt, a balanced low (high) potential temperature anomaly forms downtilt (uptilt). The mesoscale lifting shifts to the right-of-tilt direction as the axisymmetric vortex flow interacts with the temperature anomaly. In the moist context, the balanced mesoscale lifting organizes convection (e.g., Davis et al. 2008). In a numerical examination of this mechanism, Braun et al. (2006) identified a wavenumber-1 potential temperature anomaly within the eyewall consistently aligned along the hurricane tilt direction. They did not find strong evidence of enhanced ascent in the right-of-tilt direction. Rather, enhanced ascent was always tied to the downtilt direction (see also examples in Rogers et al. 2003; Zhu et al. 2004; Wu et al. 2006; Davis et al. 2008). The orientation of the peak composite vertical motion in Fig. 10 supports this relationship between tilt and enhanced convection.

Another explanation for the shear-induced convective asymmetry relates convective organization to vorticity balance on the vortex scale (Willoughby et al. 1984; Bender 1997; Frank and Ritchie 2001). According to this argument, the tendency for vortex stretching to balance radial advection of vorticity requires low-level convergence and ascent where the low-level, storm-relative asymmetric flow approaches the eyewall. Based upon the orientation of the storm-relative asymmetric flow in Fig. 9b, the greatest negative (positive) radial advective tendency at low levels should occur within the DSR (USL) quadrant. Figure 9b also indicates a wavenumber-1 structure in the composite divergence field of the eyewall such that the positive (negative) stretching tendency is skewed toward the DSR (USL) quadrant, confirming the opposing tendency of these two terms in the vorticity budget. Although the peak composite ascent falls more closely in the downshear/downtilt direction (cf. Fig. 10), the skewing of the composite ascent distribution to the DSR is qualitatively consistent with the vorticity balance argument.

Figure 10 shows that the peak composite reflectivity at 2 km occurs immediately downwind of the greatest composite midlevel ascent. This observation suggests that convective cells grow and mature as they rotate through the downshear semicircle following their initiation within the DSR to thedownshear region of the eyewall. Black et al. (2002) observed the occurrence of reflectivity values >40 dBZ below the axis of individual deep updrafts in the DSL quadrant, indicating a mature stage of convection in which collision–coalescence processes had sufficient time to produce large hydrometeors. Through a multicase statistical study of Tropical Rainfall Measuring Mission (TRMM) Precipitation Radar data, Hence and Houze (2011) confirmed the presence of younger convection DSR and a more mature mixture of intense convective and stratiform echo DSL.

Figure 10 also shows that descent dominates the composite vertical motion at 5 km in the USL eyewall. According to the aforementioned vorticity balance arguments, mesoscale descent is favored where the storm-relative flow exits the low-level eyewall region and deep divergence occurs (i.e., USL in Fig. 9b). Precipitation falling into this quadrant may produce locally stronger downdrafts through evaporative cooling and condensate loading (Black et al. 2002; Eastin et al. 2005). The USR quadrant contains the weakest eyewall echoes since most precipitation has fallen out of the cyclonically ascending updrafts, and parcels must circle some distance before they reach the region where mesoscale ascent,

and the stimulation of vigorous convection, is again favored. The precise location where new convection initiates may depend in part on the ability of surface heat fluxes to provide air parcels orbiting through the upshear side of the eyewall with sufficient values of θ_e (Eastin et al. 2005; Zhang et al. 2013). The internal dynamics and thermodynamics associated with vorticity asymmetry rotating about the eyewall may also modulate this location (Eastin et al. 2005; Braun et al. 2006; Reasor et al. 2009).

Within the vortex skirt region, Fig. 10 shows elevated reflectivity and ascent extending radially outward from the eyewall in the DSL quadrant, and a band of enhanced ascent surrounding the eyewall in the downshear semicircle. These structures resemble the stationary band complex in the near-core region documented by Willoughby et al. (1984) and, more recently, Riemer et al. (2010). This shear-relative band structure is supported in several of the individual cases when examined over their full domain (not shown). On the upshear side, descending motion dominates outside the eyewall and contributes to a wavenumber-1 pattern of vertical motion within the vortex skirt. Depressed values of reflectivity are observed primarily in the USR quadrant from $r^* = 1$–2.5 and connect to the weak echo region of the eyewall in the same quadrant.

The three-dimensional structure of the shear-relative composite hurricane is conveyed in Fig. 11 through radius–height cross sections of quadrant-average reflectivity, radial velocity, and vertical velocity. In the DSR quadrant, low-level (<4 km) eyewall ascent is, on average, at least twice as large as the ascent in the upwind USR quadrant and slightly stronger than found in the DSL quadrant. These composite observations of the low-level eyewall further support the DSR quadrant as the typical location of convective initiation. This quadrant also contains the deepest inflow within the core region, and, as discussed above, is the location where the storm-relative asymmetric flow is directed inward toward the eyewall.

In the DSL quadrant, the composite eyewall ascent is as deep as that observed DSR, but is not quite as strong throughout its depth. Relative to the DSR quadrant, eyewall reflectivity is elevated throughout the troposphere. The inflow is shallower, and a more pronounced outflow maximum is present just inside $r^* = 1$ near the top of the boundary layer. Also, at middle to upper levels ($z > 4$ km), descent is present along the inner edge of the eyewall.

Consistent with the updraft life cycle described in Black et al. (2002), reflectivity values are reduced in the USL quadrant (relative to the DSL quadrant) as the remaining precipitation falls out. Parcels unloaded of precipitation accelerate vertically with the strongest ascent confined above 8 km. Low values of composite vertical motion through the lower to midtroposphere reflect the preponderance of downdrafts in the USL quadrant noted by Black et al. (2002). Inflow within the USL quadrant is either nonexistent or confined below the 0.5-km height, the lowest level of the Doppler wind analysis. A deep layer of outflow at $r^* = 1$ extends to approximately 3.5-km height.

By the time cells rotate into the USR quadrant, most precipitation has already fallen out, resulting in the weakest low-level echoes in the shear-relative eyewall. Composite vertical motion within the eyewall is once again nonnegligible and positive within the lower to middle troposphere, suggesting some convective initiation there. The low-level inflow, if it exists, remains confined below 0.5-km height, with a shallower outflow overlain by deep inflow.

c. *Shear-relative hurricane: Low versus high shear*

The significance of the structures documented in the shear-relative composite is assessed by considering low- ($<4\,\mathrm{m\,s^{-1}}$, mean $2.1\,\mathrm{m\,s^{-1}}$) and high- ($>7\,\mathrm{m\,s^{-1}}$, mean $8.7\,\mathrm{m\,s^{-1}}$) shear stratifications (Table 1). The low-shear stratification includes cases for which the shear is less than $2.5\,\mathrm{m\,s^{-1}}$. As in Fig. 11, quadrant averages of fields were constructed from the low- (Fig. 12) and high- (Fig. 13) shear composites. The difference between the composite means (high minus low shear) is shown explicitly in Fig. 14. Structural differences significant at the 95% confidence level are emphasized using the structure metrics defined in Table 2.

The low-shear composite (Fig. 12) is visibly axisymmetric, although a slight upshear–downshear asymmetry is present even at these small shear magnitudes. Otherwise, the cross sections in individual quadrants resemble the axisymmetric composite in Rogers et al. (2012, their Figs. 7 and 8). The more weakly sheared hurricanes are generally characterized in all quadrants by inflow within the lowest few kilometers, strongest ascent confined to a narrow radial band near $r^* = 1$, strongest resolved outflow coinciding with the upper-level ascent maximum, and, on average, weak subsidence immediately outside the eyewall.

The radial flow structure at high-shear values (Fig. 13) is similar to that for the entire database (Fig. 11), but with a larger magnitude upper-level flow. The lower- and upper-level differences between the high- and low-shear composites of radial flow outside $r^* = 1$ in the DSR and USL quadrants are statistically significant (Fig. 14; Table 2). Recall from the discussion of Fig. 9 that the asymmetric component of the radial flow outside $r^* = 1$ is largely accounted for by the storm-relative flow entering (exiting) the eyewall in the DSR (USL)

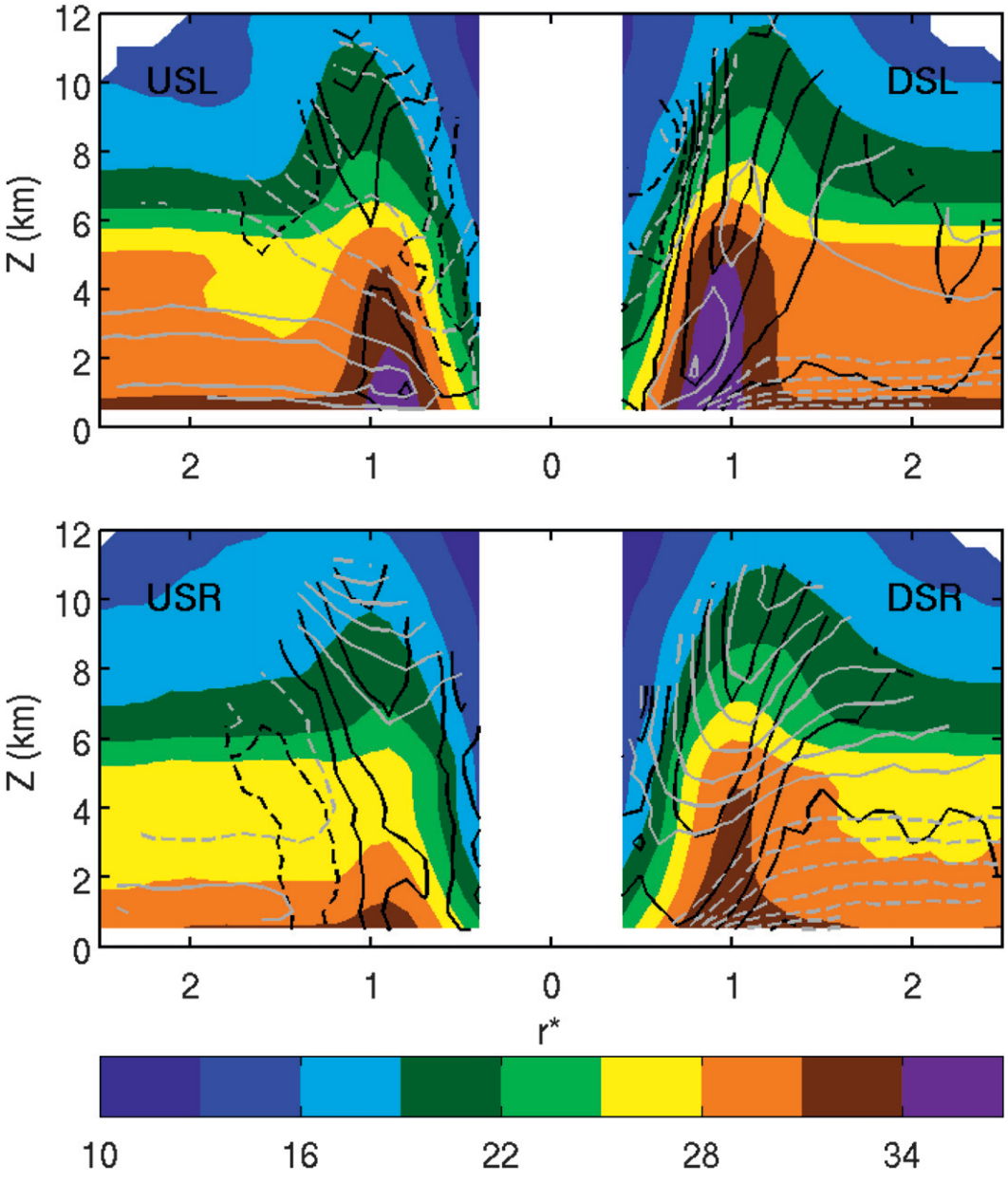

FIG. 11. Quadrant-average cross sections of shear-relative composite reflectivity (dBZ, shaded), vertical velocity ($m\,s^{-1}$, black contours), and radial velocity ($m\,s^{-1}$, gray contours) for cases with $V_{max} > 31\,m\,s^{-1}$ and $S_{850-200} > 2.5\,m\,s^{-1}$. The quadrants are arranged such that the shear vector points to the right of the page. Regions of negative vertical motion are highlighted by the 0 and $-0.25\,m\,s^{-1}$ dashed black contours. Contours of positive vertical motion (solid black) are drawn at 0.25, 0.5, 1, 1.5, 2, and $2.5\,m\,s^{-1}$. The contour interval for radial inflow (dashed gray) and outflow (solid gray) is $1\,m\,s^{-1}$ (zero contour omitted). The radial coordinate r^* is scaled by RMW_{2km}.

quadrant at low levels. The reverse is true at upper levels. This significant change in the radial flow confirms that increases in shear magnitude on the large scale are manifest on the more local scale of the core region.

The azimuthal asymmetry in eyewall convection is enhanced with increased shear magnitude. Overall, the reflectivity distribution of the high-shear composite shown in Fig. 13 resembles that for the entire database (Fig. 11). Greater shear forcing produces a statistically significant suppression of eyewall reflectivity within the right-of-shear semicircle, with the largest difference occurring USR (Fig. 14; Table 2). Figure 14 suggests that the reduced precipitation USR is likely a consequence

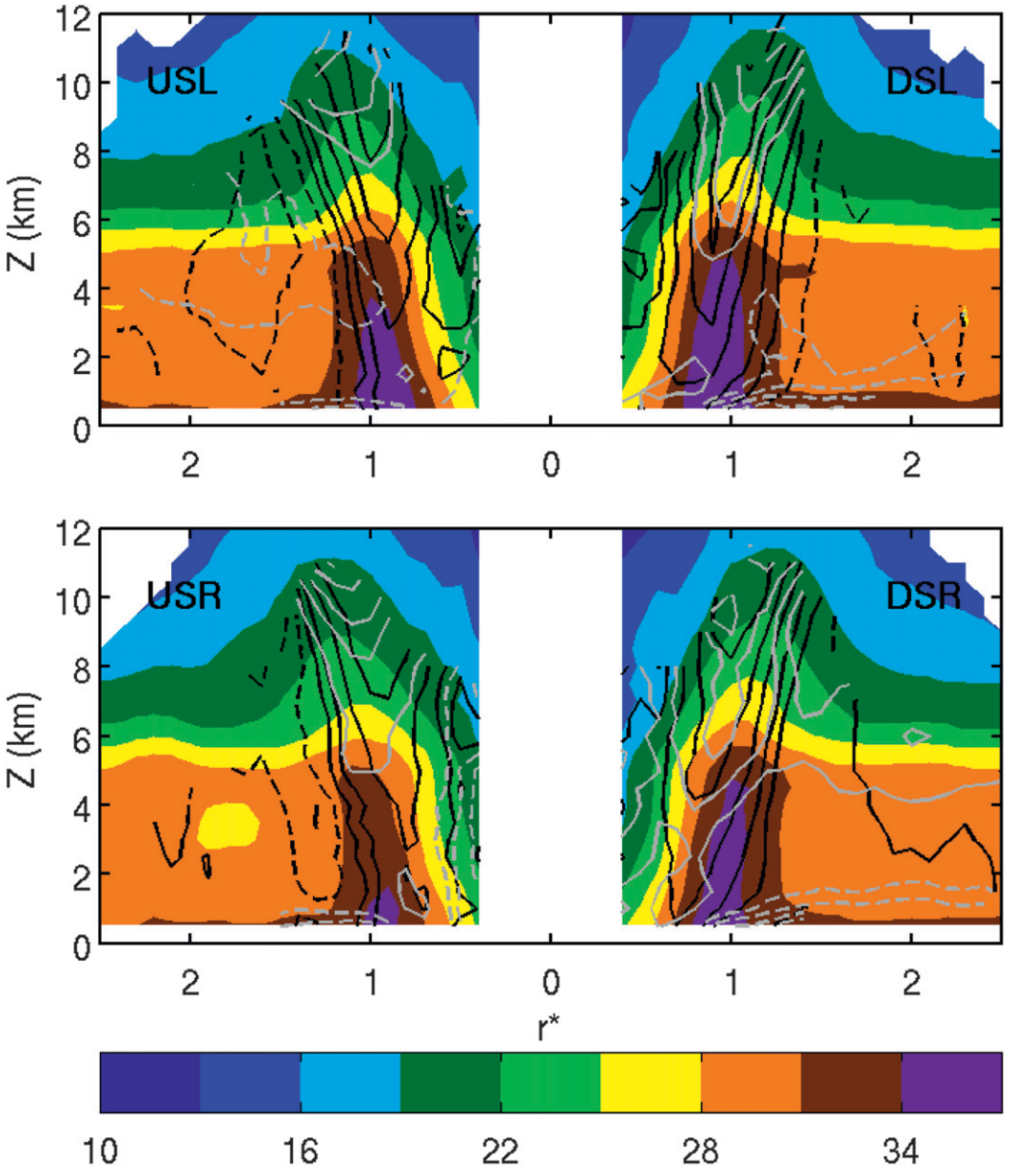

FIG. 12. As in Fig. 11, but for the low-shear stratification of cases with $V_{max} > 31\,m\,s^{-1}$ and $S_{850-200} < 4\,m\,s^{-1}$.

of diminished eyewall ascent upwind in the USL quadrant. Comparison of Figs. 12 and 13 shows that eyewall ascent in the USL quadrant is actually replaced by weak descent through a deep layer of the lower to midtroposphere at higher shear. This change in USL eyewall vertical velocity is also statistically significant (Table 2). A close examination of Fig. 14 reveals that the suppression of reflectivity extends upwind into the USL quadrant, but radially outside $r^* = 1$. The statistical significance of this difference has been confirmed (not shown). The radially inward shifting of suppressed reflectivity from the USL to DSR quadrants is consistent with the inward spiraling of an upshear weak-echo band, as documented by Reasor et al. (2009, their Fig. 6) in vertically sheared Hurricane Guillermo (1997).

In contrast, the downshear side of the eyewall shows structural changes that may be consistent with enhanced convective intensity. Within the DSR quadrant, increased shear leads to a statistically significant increase in ascent through a deep layer of the eyewall (Fig. 14; Table 2). Comparison of Figs. 12 and 13 shows that this increase within the $r^* = 0.6$–1.2 band results from an increase in

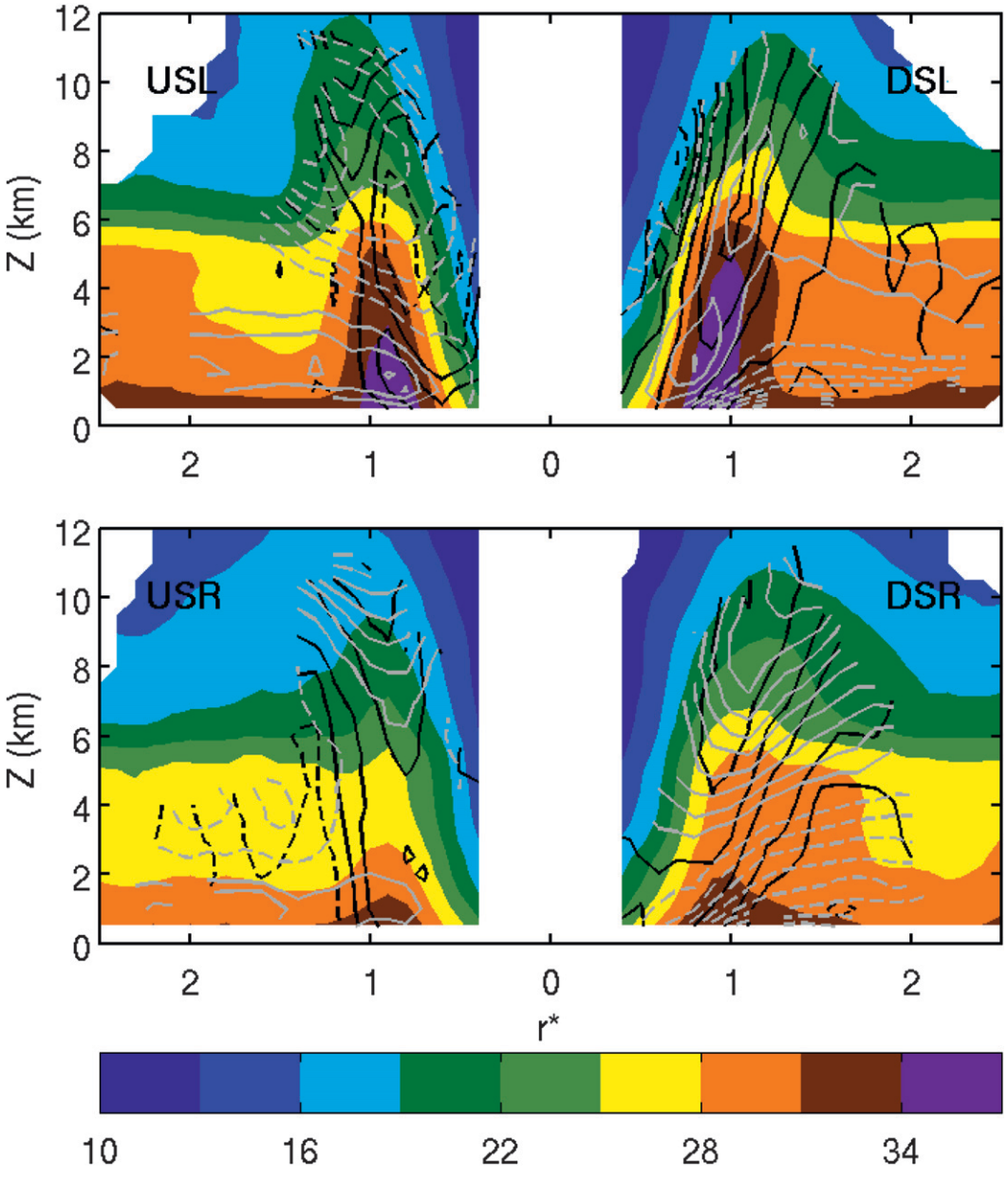

FIG. 13. As in Fig. 11, but for the high-shear stratification of cases with $V_{max} > 31\,m\,s^{-1}$ and $S_{850-200} > 7\,m\,s^{-1}$.

magnitude, and radially outward shifting, of peak composite eyewall ascent. In the DSL quadrant of the eyewall, Fig. 14 indicates that higher shear yields stronger low-level inflow and a statistically significant deeper low-level outflow inside $r^* = 1$ (Table 2). Also at higher shear, resolved descent is observed along the inner edge of the eyewall above 6 km (Fig. 13). Recent and prior studies have shown that the most vigorous updrafts are commonly observed in the DSL quadrant (Rogers et al. 2013), and tend to have the most buoyant cores within the eyewall (Eastin et al. 2005). While Fig. 13 reveals a DSL eyewall structure that is consistent with the presence of buoyant convection (e.g., deep inflow and enhanced eye subsidence from convective detrainment), it is not yet clear whether the aforementioned differences in composite structure between Figs. 12 and 13 point to an enhancement of updraft core buoyancy with increased shear strength. Future analysis of the convective statistics similar to Eastin et al. (2005) and Rogers et al. (2013), but for the low- and high-shear stratifications, is necessary to fully address the question of how the shear forcing strength impacts the characteristics of eyewall convection.

Outside the eyewall, within the vortex skirt, the most statistically significant impact of shear is on lower- to

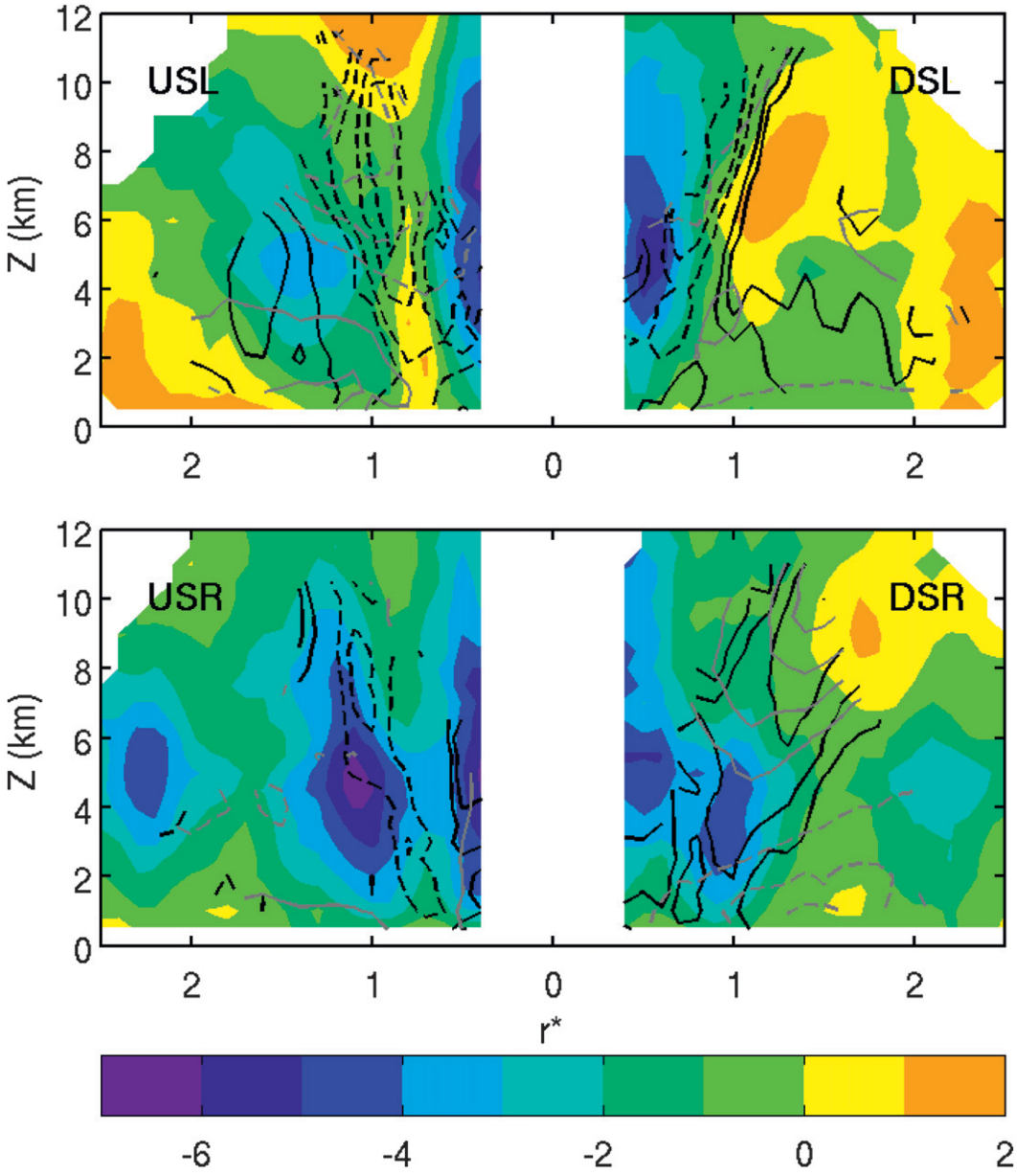

FIG. 14. Difference (high minus low shear) between the shear-relative composite mean reflectivity (dBZ, shaded), vertical velocity ($m\,s^{-1}$, black contours), and radial velocity ($m\,s^{-1}$, gray contours) shown in Figs. 12 and 13. Contours of positive (solid black) and negative (dashed black) vertical velocity difference are drawn at ±0.25, ±0.5, ±1, ±1.5, and ±2 $m\,s^{-1}$. The contour interval for positive (solid gray) and negative (dashed gray) radial flow difference is 2 $m\,s^{-1}$ (zero contour omitted). The radial coordinate r^* is scaled by RMW_{2km}.

midtropospheric vertical motion within the semicircle left of shear, and on reflectivity in the USR quadrant (Fig. 14; Table 2). The positive difference in vertical motion arises as weak descent outside the eyewall in the low-shear composite (Fig. 12) is replaced by weak ascent at higher values of shear (Fig. 13). The shear-relative band of ascent outside the DSL eyewall between $r^* = 1.4$–2, observed in the 5-km vertical motion field of the total composite (Fig. 10), is also present in the high-shear composite (not shown). The reduced reflectivity within the USR quadrant of the skirt is likely due to upshear suppression of convective rainbands in the higher-shear environment.

d. *Motion-relative hurricane structure*

The leading-order impact of uniform translational flow upon hurricane structure results from asymmetries in surface friction within the boundary layer (Shapiro

TABLE 2. Differences (high minus low shear) in area-average structure metrics derived from the composite means (see Figs. 12 and 13) in each shear-relative quadrant. A one-tailed Student's *t* test was performed, and differences between composites significant at >95% are set boldface. The radial coordinate r^* is scaled by RMW_{2km}.

	Radial band	Depth (km)	DSR	DSL	USL	USR
Low-level radial flow ($m\,s^{-1}$)	$1 < r^* < 2$	0.5–2	**−4.1**	−1.3	**2.5**	1.7
Upper-level radial flow ($m\,s^{-1}$)	$1 < r^* < 2$	6–10	**4.5**	0.5	**-5.5**	−0.7
Eyewall reflectivity (dB*Z*)	$0.8 < r^* < 1.2$	3–6	**−3.8**	−0.3	−0.9	**−4.7**
Eyewall vertical velocity ($m\,s^{-1}$)	$0.6 < r^* < 1.2$	3.5–6.5	**0.6**	−0.0	**-0.8**	−0.2
Low-level eyewall outflow ($m\,s^{-1}$)	$0.8 < r^* < 1$	2.5–3.5	−0.6	**2.0**	0.6	−0.6
Skirt reflectivity (dB*Z*)	$2 < r^* < 2.5$	3–6	−1.9	0.9	0.3	**−3.3**
Skirt vertical velocity ($m\,s^{-1}$)	$1.4 < r^* < 2$	2–6	0.1	**0.5**	**0.4**	−0.1

1983; Kepert 2001; Kepert and Wang 2001). In the idealized numerical experiments of Shapiro (1983) without convection and with prescribed flow above the hurricane boundary layer, convergence is enhanced on the forward side of the vortex with respect to the motion. Recently, the impact of translation on hurricane structure has been revisited by Thomsen et al. (2013, manuscript submitted to *Mon. Wea. Rev.*) in the context of relatively high resolution, convection-permitting numerical experiments. For hurricanes stronger than those considered by Shapiro (1983) and at the fastest translation speed considered ($7.5\,m\,s^{-1}$), a robust asymmetry in eyewall vertical motion was found with peak ascent located approximately 45° left of motion.

In documenting the motion impacts on hurricane asymmetry using the Doppler radar database, we must consider the finding of CM3 that convective asymmetry is highly correlated with the vertical wind shear. As they note, composites relative to motion may simply reflect the impacts of shear since a preferred relationship between the direction of motion and the direction of deep-layer shear typically exists. One method for diagnosing motion impacts is to stratify cases according to both translational speed and shear magnitude such that only low-shear values are considered in slow- and fast-motion composites. For the current radar database, only 11 cases have shear values less than $2.5\,m\,s^{-1}$, and of those the translational speed is limited to a range of $2–6.5\,m\,s^{-1}$. The method employed here seeks to isolate the impacts of motion by considering only those cases where the front quadrant and downshear quadrant are sufficiently distinct. Figure 15 shows the direction of motion and shear for each of the cases with $V_{max} > 31\,m\,s^{-1}$. Two composites are created, one in which the shear direction is between 90° and 180° to the right of motion, and the other in which the shear direction is between 90° and 180° to the left of motion (Table 1).

The motion-relative composites of convective structure shown in Fig. 16 indicate that the predominant eyewall asymmetry remains closely associated with the vertical wind shear. In Fig. 16a, the peak composite ascent falls along the downwind edge of the quadrant containing the shear vector. The peak composite ascent in Fig. 16b spans the quadrant containing the shear vector. In both cases, the region of elevated composite reflectivity is observed downwind of this quadrant. On the upshear side of the eyewall there is some indication of descent near the trailing edge of the elevated reflectivity, but this is not followed by weak vertical motion downwind, as in the shear-relative composites. Instead, a secondary maximum in eyewall ascent is observed 45° left of motion in Fig. 16a and in the direction of motion in Fig. 16b. The former maximum also coincides with a secondary maximum in reflectivity. Given the relatively small sample sizes used to construct these motion-relative composites, it is difficult to assess the statistical significance of the secondary features, or whether they have any relationship to the motion. As the

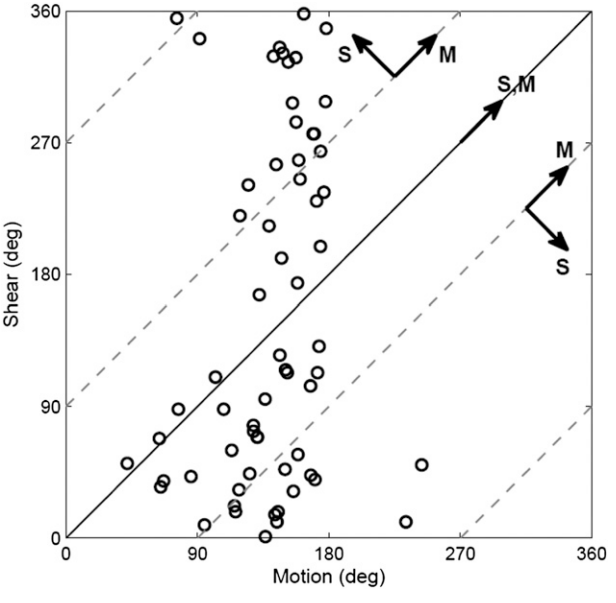

FIG. 15. Direction of storm motion ("M") and 850–200-hPa shear ("S") for cases with $V_{max} > 31\,m\,s^{-1}$. The standard mathematical convention is used for angles (i.e., 90° = N, 0° = E, etc.). Cases falling along the diagonal have storm motion in the same direction as the large-scale shear. Cases falling 90° off the diagonal have orthogonal motion and shear vectors.

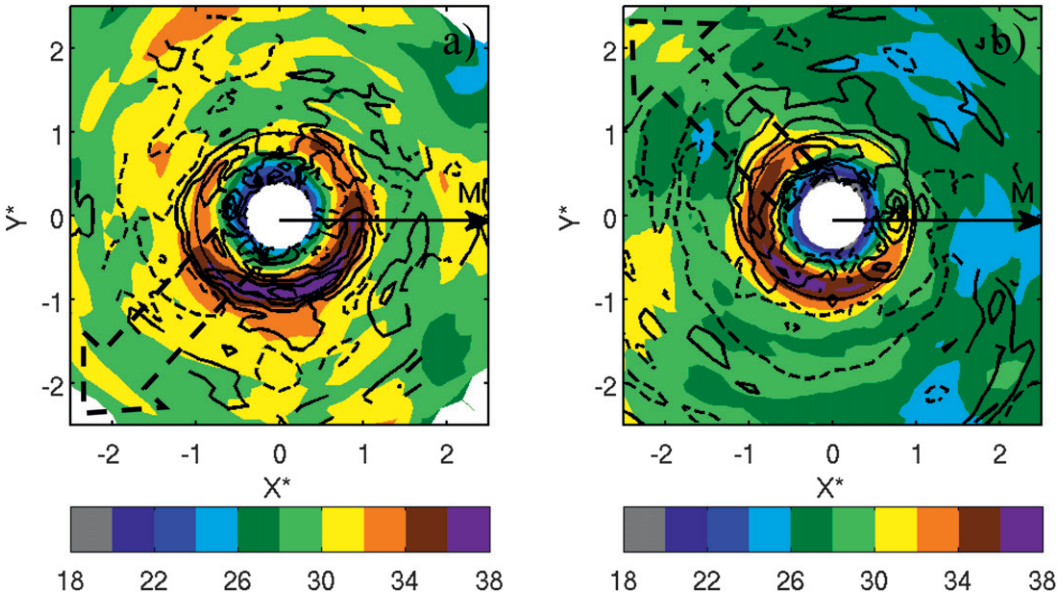

FIG. 16. Motion-relative composite of 2-km reflectivity (dBZ, shaded) and 5-km vertical velocity ($m\,s^{-1}$, contour) for cases with $V_{max} > 31\ m\,s^{-1}$ and in which the shear vector points 90°–180° to the (a) right and (b) left of the motion direction indicated by "M". The heavy dashed arrows indicate the quadrant containing the shear vector. Negative values of vertical velocity are bounded by the dashed contour. Positive values (solid) are contoured from $0.5\ m\,s^{-1}$ at an interval of $0.5\ m\,s^{-1}$. Horizontal distance (X^*, Y^*) is scaled by RMW_{2km} with $r^* = 1$ denoted by the circle.

radar database is expanded, we should be able to draw greater inferences from such stratifications.

4. Conclusions

The asymmetric structure of hurricane-strength TCs has been examined using a database of Doppler radar observations collected during 75 NOAA WP-3D aircraft flights over the past two decades. Of particular interest here is the component of vortex asymmetry forced by the storm's interaction with its environmental flow. For the first time, the three-dimensional, shear-relative kinematic asymmetry of observed hurricanes is documented through a composite approach, similar to that employed previously for the lightning and precipitation fields. The statistical significance of the shear-relative structure was assessed through an analysis of low- and high-shear stratifications. A stratification of results according to motion and shear direction largely confirmed the predominant impact of shear forcing over motion forcing on the vortex-scale asymmetry above the boundary layer. An expansion of the database to include a wider range of shear magnitudes and translation speeds will be necessary to further investigate the relative roles of shear and motion in influencing the structure of observed storms.

Vertical wind shear impacts hurricane structure in several ways. First, differential advection tilts the vortex in the direction of the large-scale shear. Relative to a local estimate of shear from the radar analyses, the tilt is oriented distinctly to the left of shear, as is common in convection-permitting numerical simulations of sheared hurricanes (Wang and Holland 1996; Rogers et al. 2003; Braun et al. 2006; Wu et al. 2006; Davis et al. 2008; Riemer et al. 2010). The tilt magnitude, however, does not show a strong relationship to the strength of the vertical wind shear. This observation has two possible explanations: 1) since tilt evolves as a vortex encounters vertical shear, and a vortex can even realign under sustained shear (Reasor et al. 2004; Jones 2004; Riemer et al. 2010), the analysis is not guaranteed to capture the vortex at its point of greatest tilt; and 2) the tilt metric used here emphasizes the core, which is typically more upright than the broader-scale vortex (Jones 1995; Reasor et al. 2004). Comparison of the perturbation vorticity field (relative to the low-level center) for low- and high-shear stratifications indeed reveals a more significant upper-level wavenumber-1 asymmetry within the eyewall at higher shear (not shown). Thus, center estimates based upon the vorticity centroid (which is not easily estimated with irregularly distributed radar data) would potentially reveal a stronger correlation between vortex tilt and shear strength.

Vertical wind shear also impacts the convective structure of the hurricane core region. Overall, the shear-relative structure of the composite hurricane agrees with

the schematic illustration of convective asymmetry presented by Black et al. (2002). The peak composite ascent is closely aligned with the downtilt direction, suggesting that balance mechanisms for forced ascent (e.g., Jones 1995) may govern to some extent the convective asymmetry of sheared hurricanes. At the same time, the composite ascent is skewed toward the DSR quadrant where the low-level inflow is deepest. A wavenumber-1 divergence pattern within the eyewall, oriented along the storm-relative asymmetric flow, also lends support to a vorticity balance argument (i.e., between radial advection and stretching of vorticity) invoked in prior studies (e.g., Bender 1997) to explain the shear-induced convective asymmetry. From an observational perspective, parallel thermodynamic composites, like that presented in RE12 for a single storm, are necessary to address the forcing mechanisms more completely. We also advocate future idealized numerical studies, motivated by the observations herein, to definitively determine the principal mechanisms for generating the shear-induced convective asymmetry of mature hurricanes.

Downwind of the DSR region of convective initiation we observe the deepest extent of high reflectivity, deep low-level inflow, a low-level outflow maximum within the eyewall, and mid- to upper-tropospheric descent along the inner edge of the eyewall. These features of the DSL quadrant are consistent with the presence of strong, buoyant updraft cores in the eyewall observed by Black et al. (2002) and Eastin et al. (2005). Demonstrating a possible source for the enhanced buoyancy, Cram et al. (2007) explicitly showed that the greatest mixing of high-θ_e air from the low-level eye into the eyewall of their simulated hurricane occurred within the DSL quadrant. Farther downwind in the USL quadrant, sinking motion is prevalent within the eyewall at lower- to midtropospheric levels. While dynamical forcing may condition this region toward descent (e.g., Jones 1995), evaporative cooling and condensate loading are more likely to guide the precise location and structure of observed descending motion (Black et al. 2002). Composite radar echoes in the USR eyewall are significantly weaker than in any other quadrant. Parcels apparently must move into the region where mesoscale ascent is preferred in the DSR quadrant before convection is stimulated. The precise location of convective initiation may also depend on the ability of surface heat fluxes to provide air parcels orbiting through the upshear side with sufficient values of θ_e (Eastin et al. 2005; Zhang et al. 2013), and on the internal dynamics and thermodynamics associated with vorticity asymmetry rotating about the eyewall (Eastin et al. 2005; Braun et al. 2006; Reasor et al. 2009).

Forthcoming work will address the representation of sheared hurricane structure in forecast models as well. In particular, parallel composite analyses of the kinematic and thermodynamic structure of sheared hurricanes will be performed using the operational Hurricane Weather Research and Forecasting Model (HWRF) (Gopalakrishnan et al. 2012). With the composite analyses presented herein as a reference, the ability of the model to reproduce a similar average shear-relative structure will be assessed. With a greater sample size from the numerical database, including a broader range of shear values and intensities, more physically meaningful stratifications may also be explored. For example, Riemer and Montgomery (2011) demonstrated that the relevant parameter governing the degree to which a TC is able to thermodynamically isolate itself from its environment involves the ratio of the shear magnitude to the vortex strength. This ratio also appears as a critical parameter in studies of vortex resilience in shear (Reasor et al. 2004).

The radar-based, shear-relative composite approach presented here is useful for future endeavors involving not only structure analysis, but also the greater intensity change problem. Rogers et al. (2013) recently used the Doppler radar database in an investigation of hurricane structure stratified by intensity change. They found that the shear-relative composite reflectivity for intensifying storms exhibits greater symmetry within the eyewall than observed for steady-state storms, despite similar mean shear. The intensifying (steady state) storms also showed a preference for convective bursts radially inside (outside) the RMW. With regards to shear-induced intensity modification, further stratification of cases, for example, according to tilt magnitude and intensity change is required to test for key structural features of proposed mechanisms. Complementary approaches using data sources that 1) offer insight into the TC's thermodynamic structure and 2) sample regions where the radar is of more limited use (e.g., the boundary layer) are also needed to fully address these proposed mechanisms. Zhang et al. (2013) recently performed a shear-relative composite analysis of the thermodynamic structure of the hurricane boundary layer using dropwindsonde data. Future work will combine the radar and dropwindsonde approaches to target cases more closely conforming to the canonical problem of a hurricane suddenly encountering vertical wind shear, as described in Riemer et al. (2010) and other idealized studies.

Acknowledgments. We thank Altuğ Aksoy, Jun Zhang, Michael Riemer, Yuqing Wang, and one anonymous reviewer for their beneficial comments that have improved the presentation and discussion of results. We thank John

Gamache whose efforts in developing and maintaining the automated software used to quality control and analyze the Doppler radar data have greatly facilitated this multicase endeavor. We are also grateful for the staff of NOAA's Aircraft Operation Center whose countless hours of dedicated service over the 75 flights represented here have made this study possible. Funding for this work was provided by NOAA base funds through the NOAA Hurricane Forecast Improvement Project (HFIP).

REFERENCES

Bender, M. A., 1997: The effect of relative flow on the asymmetric structure in the interior of hurricanes. *J. Atmos. Sci.,* **54,** 703–724.

Black, M. L., J. F. Gamache, F. D. Marks, C. E. Samsury, and H. E. Willoughby, 2002: Eastern Pacific Hurricanes Jimena of 1991 and Olivia of 1994: The effect of vertical shear on structure and intensity. *Mon. Wea. Rev.,* **130,** 2291–2312.

Braun, S. A., and L. Wu, 2007: A numerical study of Hurricane Erin (2001). Part II: Shear and the organization of eyewall vertical motion. *Mon. Wea. Rev.,* **135,** 1179–1194.

——, M. T. Montgomery, and Z. Pu, 2006: High-resolution simulation of Hurricane Bonnie (1998). Part I: The organization of eyewall vertical motion. *J. Atmos. Sci.,* **63,** 19–42.

Cecil, D. J., 2007: Satellite-derived rain rates in vertically sheared tropical cyclones. *Geophys. Res. Lett.,* **34,** L02811, doi:10.1029/2006GL027942.

Chen, S. Y. S., J. A. Knaff, and F. D. Marks, 2006: Effects of vertical wind shear and storm motion on tropical cyclone rainfall asymmetries deduced from TRMM. *Mon. Wea. Rev.,* **134,** 3190–3208.

Corbosiero, K. L., and J. Molinari, 2002: The effects of vertical wind shear on the distribution of convection in tropical cyclones. *Mon. Wea. Rev.,* **130,** 2110–2123.

——, and ——, 2003: The relationship between storm motion, vertical wind shear, and convective asymmetries in tropical cyclones. *J. Atmos. Sci.,* **60,** 366–376.

Cram, T. A., J. Persing, M. T. Montgomery, and S. A. Braun, 2007: A Lagrangian trajectory view on transport and mixing processes between the eye, eyewall, and environment using a high-resolution simulation of Hurricane Bonnie (1998). *J. Atmos. Sci.,* **64,** 1835–1856.

Davis, C. A., S. C. Jones, and M. Riemer, 2008: Hurricane vortex dynamics during Atlantic extratropical transition. *J. Atmos. Sci.,* **65,** 714–736.

DeMaria, M., 1996: The effect of vertical shear on tropical cyclone intensity change. *J. Atmos. Sci.,* **53,** 2076–2088.

——, M. Mainelli, L. K. Shay, J. A. Knaff, and J. Kaplan, 2005: Further improvements to the Statistical Hurricane Intensity Prediction Scheme (SHIPS). *Wea. Forecasting,* **20,** 531–543.

Dunion, J. P., and C. S. Velden, 2004: The impact of the Saharan Air Layer on Atlantic tropical cyclone activity. *Bull. Amer. Meteor. Soc.,* **85,** 353–365.

Eastin, M. D., W. M. Gray, and P. G. Black, 2005: Buoyancy of convective vertical motions in the inner core of intense hurricanes. Part II: Case studies. *Mon. Wea. Rev.,* **133,** 209–227.

Frank, W. M., and E. A. Ritchie, 2001: Effects of vertical wind shear on the intensity and structure of numerically simulated hurricanes. *Mon. Wea. Rev.,* **129,** 2249–2269.

Gamache, J. F., 1997: Evaluation of a fully three-dimensional variational Doppler analysis technique. Preprints, *28th Conf. on Radar Meteorology,* Austin, TX, Amer. Meteor. Soc., 422–423.

——, 2005: Real-time dissemination of hurricane wind fields determined from airborne Doppler radar data. National Hurricane Center, 38 pp. [Available online at http://www.nhc.noaa.gov/jht/2003-2005reports/DOPLRgamache_JHTfinalreport.pdf.]

Gopalakrishnan, S. G., Q. Liu, T. Marchok, D. Sheinin, N. Surgi, R. Tuleya, R. Yablonsky, and X. Zhang, 2012: Hurricane Weather and Research and Forecasting (HWRF) model: Scientific documentation. NOAA/NCAR/Development Tech Center, 96 pp. [Available online at http://www.dtcenter.org/HurrWRF/users/docs/scientific_documents/HWRFScientificDocumentation_v3.4a.pdf.]

Hence, D. A., and R. A. Houze Jr., 2011: Vertical structure of hurricane eyewalls as seen by the TRMM Precipitation Radar. *J. Atmos. Sci.,* **68,** 1637–1652.

Jones, S. C., 1995: The evolution of vortices in vertical shear. I: Initially barotropic vortices. *Quart. J. Roy. Meteor. Soc.,* **121,** 821–851.

——, 2004: On the ability of dry tropical-cyclone-like vortices to withstand vertical shear. *J. Atmos. Sci.,* **61,** 114–119.

Kaplan, J., M. DeMaria, and J. A. Knaff, 2010: A revised tropical cyclone rapid intensification index for the Atlantic and eastern North Pacific basins. *Wea. Forecasting,* **25,** 220–241.

Kepert, J. D., 2001: The dynamics of boundary layer jets within the tropical cyclone core. Part I: Linear theory. *J. Atmos. Sci.,* **58,** 2469–2484.

——, and Y. Wang, 2001: The dynamics of boundary layer jets within the tropical cyclone core. Part II: Nonlinear enhancement. *J. Atmos. Sci.,* **58,** 2485–2501.

Knaff, J., S. Seseske, M. DeMaria, and J. Demuth, 2004: On the influences of vertical wind shear on symmetric tropical cyclone structure derived from AMSU. *Mon. Wea. Rev.,* **132,** 2503–2510.

Kossin, J. P., and W. H. Schubert, 2001: Mesovortices, polygonal flow patterns, and rapid pressure falls in hurricane-like vortices. *J. Atmos. Sci.,* **58,** 2196–2209.

Mallen, K. J., M. T. Montgomery, and B. Wang, 2005: Reexamining the near-core radial structure of the tropical cyclone primary circulation: Implications for vortex resiliency. *J. Atmos. Sci.,* **62,** 408–425.

Marks, F. D., Jr., and R. A. Houze Jr., 1987: Inner core structure of Hurricane Alicia from airborne Doppler radar observations. *J. Atmos. Sci.,* **44,** 1296–1317.

——, ——, and J. F. Gamache, 1992: Dual-aircraft investigation of the inner core of Hurricane Norbert. Part I: Kinematic structure. *J. Atmos. Sci.,* **49,** 919–942.

May, P. T., and G. J. Holland, 1999: The role of potential vorticity generation in tropical cyclone rainbands. *J. Atmos. Sci.,* **56,** 1224–1228.

Molinari, J., and D. Vollaro, 2010: Distribution of helicity, CAPE, and shear in tropical cyclones. *J. Atmos. Sci.,* **67,** 274–284.

Montgomery, M. T., and R. J. Kallenbach, 1997: A theory for vortex Rossby waves and its application to spiral bands and intensity changes in hurricanes. *Quart. J. Roy. Meteor. Soc.,* **123,** 435–465.

Nguyen, M. C., M. J. Reeder, N. E. Davidson, R. K. Smith, and M. T. Montgomery, 2011: Inner-core vacillation cycles during the intensification of Hurricane Katrina. *Quart. J. Roy. Meteor. Soc.,* **137,** 829–844.

Nguyen, V. S., R. K. Smith, and M. T. Montgomery, 2008: Tropical cyclone intensification and predictability in three dimensions. *Quart. J. Roy. Meteor. Soc.,* **134,** 563–582.

Nolan, D. S., M. T. Montgomery, and L. D. Grasso, 2001: The wavenumber-one instability and trochoidal motion of hurricane-like vortices. *J. Atmos. Sci.,* **58,** 3243–3270.

Reasor, P. D., and M. T. Montgomery, 2001: Three-dimensional alignment and corotation of weak, TC-like vortices via linear vortex Rossby waves. *J. Atmos. Sci.,* **58,** 2306–2330.

——, and M. D. Eastin, 2012: Rapidly intensifying Hurricane Guillermo (1997). Part II: Resilience in shear. *Mon. Wea. Rev.,* **140,** 425–444.

——, M. T. Montgomery, F. D. Marks Jr., and J. F. Gamache, 2000: Low-wavenumber structure and evolution of the hurricane inner core observed by airborne dual-Doppler radar. *Mon. Wea. Rev.,* **128,** 1653–1680.

——, ——, and L. D. Grasso, 2004: A new look at the problem of tropical cyclones in vertical shear flow: Vortex resiliency. *J. Atmos. Sci.,* **61,** 3–22.

——, M. Eastin, and J. F. Gamache, 2009: Rapidly intensifying Hurricane Guillermo (1997). Part I: Low-wavenumber structure and evolution. *Mon. Wea. Rev.,* **137,** 603–631.

Reynolds, R. W., and T. M. Smith, 1993: An improved real-time global sea surface temperature analysis. *J. Climate,* **6,** 114–119.

Riemer, M., and M. T. Montgomery, 2011: Simple kinematic models for the environmental interaction of tropical cyclones in vertical wind shear. *Atmos. Chem. Phys.,* **11,** 9395–9414.

——, ——, and M. E. Nicholls, 2010: A new paradigm for intensity modification of tropical cyclones: Thermodynamic impact of vertical wind shear on the inflow layer. *Atmos. Chem. Phys.,* **10,** 3163–3188.

Rogers, R., S. S. Chen, J. E. Tenerelli, and H. E. Willoughby, 2003: A numerical study of the impact of vertical shear on the distribution of rainfall in Hurricane Bonnie (1998). *Mon. Wea. Rev.,* **131,** 1577–1599.

——, and Coauthors, 2006: The Intensity Forecasting Experiment: A NOAA multiyear field program for improving tropical cyclone intensity forecasts. *Bull. Amer. Meteor. Soc.,* **87,** 1523–1537.

——, S. Lorsolo, P. Reasor, J. Gamache, and F. Marks, 2012: Multiscale analysis of tropical cyclone kinematic structure from airborne Doppler radar composites. *Mon. Wea. Rev.,* **140,** 77–99.

——, P. Reasor, and S. Lorsolo, 2013: Airborne Doppler observations of the inner-core structural differences between intensifying and steady-state tropical cyclones. *Mon. Wea. Rev.,* **141,** 2970–2991.

Schecter, D. A., and M. T. Montgomery, 2007: Waves in a cloudy vortex. *J. Atmos. Sci.,* **64,** 314–337.

Schubert, W. H., M. T. Mongomery, R. K. Taft, T. A. Guinn, S. R. Fulton, J. P. Kossin, and J. P. Edwards, 1999: Polygonal eyewalls, asymmetric eye contraction, and potential vorticity mixing in hurricanes. *J. Atmos. Sci.,* **56,** 1197–1223.

Shapiro, L. J., 1983: The asymmetric boundary layer flow under a translating hurricane. *J. Atmos. Sci.,* **40,** 1984–1998.

Simpson, R. H., and H. Riehl, 1958: Mid-tropospheric ventilation as a constraint on hurricane development and maintenance. *Proc. Tech. Conf. on Hurricanes,* Miami, FL, Amer. Meteor. Soc., D4.1–D4.10.

Tang, B., and K. Emanuel, 2012: Sensitivity of tropical cyclone intensity to ventilation in an axisymmetric model. *J. Atmos. Sci.,* **69,** 2394–2413.

Ueno, M., 2007: Observational analysis and numerical evaluation of the effects of vertical wind shear on the rainfall asymmetry in the typhoon inner-core region. *J. Meteor. Soc. Japan,* **85,** 115–136.

Wang, Y., and G. J. Holland, 1996: Tropical cyclone motion and evolution in vertical shear. *J. Atmos. Sci.,* **53,** 3313–3332.

Willoughby, H. E., F. D. Marks, and R. J. Feinberg, 1984: Stationary and propagating convective bands in asymmetric hurricanes. *J. Atmos. Sci.,* **41,** 3189–3211.

Wingo, M. T., and D. J. Cecil, 2010: Effects of vertical wind shear on tropical cyclone precipitation. *Mon. Wea. Rev.,* **138,** 645–662.

Wong, M. L. M., and J. C. L. Chan, 2004: Tropical cyclone intensity in vertical wind shear. *J. Atmos. Sci.,* **61,** 1859–1876.

Wu, L., S. A. Braun, J. Halverson, and G. Heymsfield, 2006: A numerical study of Hurricane Erin (2001). Part I: Model verification and storm evolution. *J. Atmos. Sci.,* **63,** 65–86.

Zhang, J. A., R. F. Rogers, P. D. Reasor, E. W. Uhlhorn, and F. D. Marks Jr., 2013: Asymmetric hurricane boundary layer structure from dropsonde composites in relation to the environmental vertical wind shear. *Mon. Wea. Rev.,* in press.

Zhu, T., D.-L. Zhang, and F. Weng, 2004: Numerical simulation of Hurricane Bonnie (1998). Part I: Eyewall evolution and intensity changes. *Mon. Wea. Rev.,* **132,** 225–241.